Summer 2017

Testing the time dependence of slip on the western Klamath Lake fault zone, Oregon

Gunnar Speth
Western Washington University, spethg@wwu.edu

TESTING THE TIME DEPENDENCE OF SLIP ON THE WESTERN KLAMATH LAKE FAULT ZONE, OREGON

By

Gunnar Speth

Accepted in Partial Completion
Of the Requirements for the Degree
Master of Science

Kathleen L. Kitto, Dean of the Graduate School

ADVISORY COMMITTEE:

Chair, Dr. Colin Amos

Dr. Elizabeth Schermer

Dr. Doug Clark

MASTER'S THESIS

In presenting this thesis in partial fulfillment of the requirements for a master's degree at Western Washington University, I grant to Western Washington University the non-exclusive royalty-free right to archive, reproduce, distribute, and display the thesis in any and all forms, including electronic format, via any digital library mechanisms maintained by WWU.

I represent and warrant this is my original work, and does not infringe or violate any rights of others. I warrant that I have obtained written permissions from the owner of any third party copyrighted material included in these files.

I acknowledge that I retain ownership rights to the copyright of this work, including but not limited to the right to use all or part of this work in future works, such as articles or books. Library users are granted permission for individual, research and non-commercial reproduction of this work for educational purposes only. Any further digital posting of this document requires specific permission from the author.

Any copying or publication of this thesis for commercial purposes, or for financial gain, is not allowed without my written permission.

Gunnar Speth

July 19, 2017

TESTING THE TIME DEPENDENCE OF SLIP ON THE WESTERN KLAMATH LAKE FAULT ZONE, OREGON

A Thesis

Presented to

The Faculty of

Western Washington University

In Partial Fulfillment

Of the Requirements for the Degree

Master of Science

by

Gunnar Speth

July 2017

Abstract

New geomorphic mapping and cosmogenic 3He geochronology on the Western Klamath Lake fault zone in southern Oregon reveals moderate, but resolvable changes in the rate of normal-fault slip rates over the past ~170 kyr. We focus on a sequence of glacial and post-glacial surfaces that record progressive offset by the fault zone over multiple time intervals. Thirty-nine new cosmogenic ^{3}He surface exposure dates and a cosmogenic nuclide depth profile establish the first late-Pleistocene glacial chronology in the Cascade Range of Oregon and constrains the timing of the last two major glacial advances in the region at 17.6 ± 2.1 ka and 97.6 ± 12.1 ka. Additionally, these data provide an estimate for the timing of an older glacial advance, likely coincident with MIS 6. Measurements of fault scarp profiles from high resolution airborne lidar provide insights into the structure of the Klamath Basin and suggest that despite a complex surface expression, individual fault strands likely merge to a single fault at depth. These measurements, coupled with the new surface chronology, allow the reconstruction of slip rates across the Western Klamath Lake fault zone over intervals of ~10^4 – 10^5 years. Our calculations indicate dip slip rates of ~0.3 mm/yr since ~100 ka, which may represent an increase from < 0.1 mm/yr prior to ~100 ka.

Acknowledgements

This research was supported by funding from the USGS EdMap program, the Evolving Earth Foundation, the Geological Society of America, the Western Washington University Graduate School, and the Western Washington University Geology department. All lidar DEMs used for mapping and topographic analysis were obtained from the Oregon Department of Geology and Mineral Industries and collected by Watershed Sciences, Inc.

I am indebted to my committee members Colin Amos, Elizabeth Schermer, and Doug Clark for guidance and feedback throughout this project. I am grateful to Dylan Rood and Greg Balco for their assistance in sample analysis. Cosmogenic dating was performed at the CalTech noble gas lab, and the Berkeley Geochronology Center. Thanks to Kylie Esselström and Samuel Graff for their assistance in field work and preparation of samples. William Amidon, Andrew Meigs, and Greg Balco provided insightful conversation about the project. The slip rate calculator used in this project was developed by Richard Styron.

Table of Contents

List of tables

List of figures

Supplementary figures

1. Introduction

Detailed, incremental measurements of fault slip over time along a single fault zone are crucial for detecting temporal changes in fault slip. Classic models of the earthquake cycle involve constant slip rates when integrating over multiple cycles (Reid, 1910; Shimazaki and Nakata, 1980). More recent models, however, introduce the idea of time-variable slip: cycles in which long periods of quiescence are punctuated by bursts of rapid strain release often represented by earthquake clusters (Wallace, 1987; Rockwell, 2000). This model has implications for our understanding of how strain accumulates and is released along fault zones, requiring measurements of progressive displacement at multiple sites along a fault zone (Mueller, 2017). Variations in slip rate with time manifest as discrepancies between long- (~10^3-10^6 years) and short-term (10^1 years) rates of deformation have been documented for both individual faults – e.g., the Altyn Tagh fault (Cowgill et al., 2009), the Garlock fault (Dolan et al., 2016), the Wasatch fault (Friedrich et al., 2003) – and for distributed zones of plate boundary deformation – e.g., the eastern California shear zone and Walker Lane Belt (Frankel et al. 2007; Peltzer et al., 2001). Potential drivers of time-variable slip include: trade-off of slip between interacting faults (Peltzer et al., 2001; Dolan et al., 2007; Dolan et al., 2016); earthquake-triggered shear zone weakening (Oskin et al., 2008); variations in surface loading between glacial-interglacial cycles (Hetzel and Hampel, 2005); response to volcanic activity (Hampel and Hetzel, 2008); and post-seismic relaxation (Dixon et al., 2003).

Our understanding of slip rate histories, however, remains limited by the scarcity and quality of incremental fault slip measurements over multiple time intervals (e.g., Amos et al., 2013). Such inventories provide a foundation for understanding the mechanisms that drive time-variable slip. Study of slip rate through time requires sites that preserve progressive offset of

multiple generations of datable deposits or landforms. Such areas are relatively uncommon, however, and are often hindered by uncertainties associated with surface dating (Gold et al., 2011).

The West Klamath Lake fault zone (WKLFZ) in southern Oregon (Fig. 1) provides an opportunity to test the time dependence of fault slip rate because it offsets multiple generations of datable deposits. There, we employ lidar-based geologic mapping and ^{3}He cosmogenic exposure dating of offset landforms to reconstruct slip rates over four time intervals across the WKLFZ. Our geochronologic results represent only the second sequence of cosmogenically dated moraines in the Cascade Range, and the first sequence of dated moraines in the Cascade Range of Oregon. Our analysis also provides insights into the structure of the fault zone at depth, as well as the WKLFZ's role in accommodating active extension associated with ongoing rotation of the Oregon Coast crustal block.

2. The Western Klamath Lake Fault Zone

2.1 Regional Tectonic Setting

Overall dextral shear between the North American and Pacific plates, paired with oblique subduction of the Juan de Fuca plate, drives interactions between discrete crustal blocks in the western United States (Wells et al. 1998). The Klamath Basin is located in south-central Oregon at the confluence of three distinct tectonic elements: The Walker Lane to the south, the Basin and Range province to the east, and the Oregon coast block to the west (Fig. 1, inset). Although the San Andreas transform takes up most of the shear across the plate boundary south of the Mendocino triple junction, the Walker Lane Belt along a distributed network of faults in Eastern

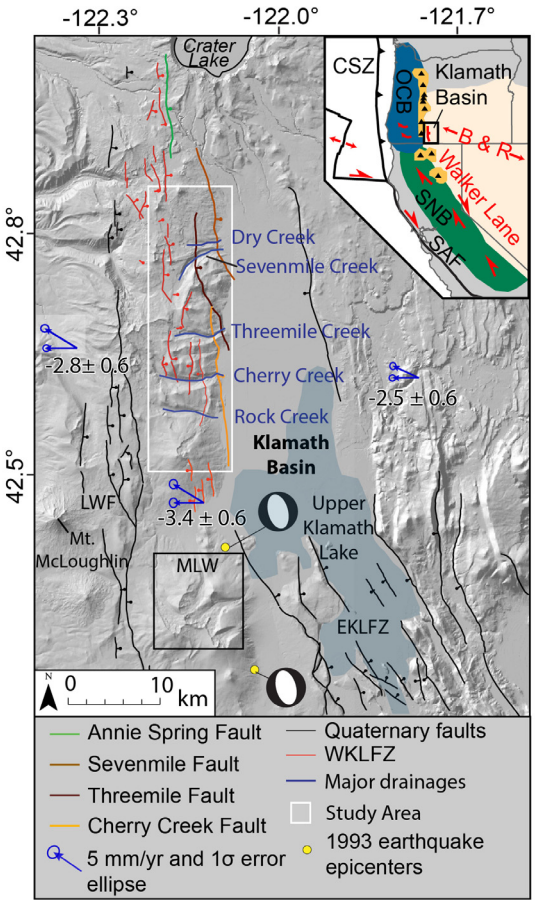

Figure 1. Overview of the Klamath Basin and the West Klamath Lake Fault Zone (WKLFZ). Basemap is a 10m DEM hillshade. The study area for this paper is enclosed in the white box. Arrows representing the average geodetic horizontal surface velocities are shown in blue (McCaffrey et al., 2013). E-W component velocities are reported in mm/yr. Locations and focal mechanisms of 1993 Mw 6.0 earthquakes from Braunmiller et al. (1995). Quaternary active fault traces from USGS (2006). Bar and ball indicate dip direction. EKLFZ - East Klamath Lake Fault Zone, LWF - Lake of the Woods Fault. MLW - Mountain Lakes Wilderness. SLW - Sky Lakes Wilderness. Inset shows relative motions of major crustal blocks along the western North American margin. Cascade arc shown in orange. Black triangles are major volcanic centers. Inset adapted from Wells et al. (1998). CSZ - Cascadia Subduction Zone, SAF - San Andreas Fault, SNB - Sierra Nevada Block; OCB – Oregon Coast Block; B&R – Basin and Range.

California (e.g., Stewart et al., 1988). Dextral shear associated Walker Lane transports the rigid Sierra Nevada block to the northwest where it collides with the Oregon coast block, resulting in the overall clockwise rotation of the Oregon coast block with respect to stable North America (Wells et al., 1998; Wells and McCaffrey, 2013). Whether dextral shear associated with the Walker Lane continues into the Cascadia backarc remains a topic of debate. One model suggests the Walker Lane terminates at the northern end of the Sierra Nevada block near the latitude of the Mendocino triple junction (Unruh et al., 2017). Other workers suggest that the pattern of en echelon northwest trending faults extending from northern California into southern Oregon represent the continuation of the Walker Lane (Pezzopone and Weldon, 1993; Blakely et al., 1997). Such northwest striking faults are connected by north striking normal faults such as the WKLFZ which represents the western boundary of the Klamath basin at the intersection of the Basin and Range province and the rotating OCB (Trench et al., 2012). The Klamath basin is actively extending

due to the rotation of the OCB, and forms part of the western boundary between the OCB and North America along the eastern margin of the Cascade arc (Fig. 1)

2.2 Quaternary geology of the WKLFZ

The Klamath basin preserves a Quaternary history of volcanism, glaciation, and lake development. The basin borders Crater Lake on the south in south central Oregon. For much of the Pleistocene the basin was filled by Pluvial Lake Modoc whose highstand was ~30 m higher than the level of present day Upper Klamath Lake (Dicken, 1980). It shrank significantly as the climate became warmer and dryer at the end of the Pleistocene, splitting into present day Upper and Lower Klamath Lakes. The northern extent of ancient Lake Modoc bordered the study area (Fig. 1) and is characterized by modern day marshes and wetlands. Pleistocene glaciers extensively modified underlying volcanic bedrock and extended into the lake, leaving behind extensive lateral moraines and outwash fans that characterize the range front today. The WKLFZ cuts these and other deposits, forming the tectonic border between the downthrown basin floor and the upthrown volcanic rocks of the Cascade Range to the west.

Volcanic activity in the Klamath basin arises from the interplay between subduction of the Juan de Fuca plate to the west and decompression melting as the result of Basin and Range extension from the east (Priest et al., 2013). The arc south of Crater Lake is characterized by a number of small shield volcanoes and isolated cinder cones (Bacon et al., 1994). Flows from these vents are generally monogenetic and basaltic-andesite in composition (Sherrod and Smith, 1990). The Burma Loop, Klamath Point, and Devils Peak shield volcanoes are the major sources for younger flows (< 1 Myr) in the study area for this project (Smith, 1988). These flows overlie

an undifferentiated unit of basaltic andesite (QTba; Fig. 2; Smith, 1988). Recent volcanic activity culminated in the climactic eruption of Mount Mazama ~7700 yr ago (Bacon, 1983). Approximately 50 km^3 of magma were erupted, with pyroclastic flows extending for tens of kilometers from their source. Much of the study area may have been covered in ash fall deposits at the time of eruption, though such deposits are only preserved today in the northern extent of the study area (Qpm; Fig. 2a), and locally in some drainages.

Shield volcanoes and associated flows have been heavily eroded by several extensive late-Pleistocene glaciations. A series of five glacially carved valleys comprise the study area. From north to south they are Dry Creek, Sevenmile Creek, Threemile Creek, Cherry Creek, and Rock Creek (Fig. 1). Several generations of glacial deposits are preserved in each valley. Deposits associated with these glaciations include till, lateral and fluted ground moraines, outwash fans and terraces, and ice-stagnation deposits. We adopt the nomenclature of Carver (1972) based on his study of the glacial deposits in the Mountain Lakes Wilderness to the south of the study area (Fig. 1). Carver (1972) correlated these deposits to the classic glacial sequence of the Sierra Nevada of California (e.g., Blackwelder, 1931). The Moss Creek stage is equivalent to the Mono Basin stage in the Sierra Nevada, the Varney Creek stage is equivalent to the Tahoe stage, and the Waban stage is equivalent to the Tioga stage at Last Glacial Maximum (LGM). Lake cores of Klamath Lake provide an estimate of 18-19 ka for the Waban (Colman et al., 2004, Reynolds et al., 2004). Direct numerical age control for the late-Pleistocene glacial sequence of the eastern Cascades is non-existent, outside of a suite of moraines dated using ^{36}Cl boulder exposure dating in Washington (Porter and Swanson, 2008). This poor age control arises in part from the absence of datable material, namely quartz which is the target for traditional ^{10}Be exposure dating. Basalt – basaltic andesite bedrock in the area, although lacking quartz, contains

abundant olivine and pyroxene, making it an ideal candidate for ^{3}He cosmogenic exposure dating of moraine crest and fan boulders (e.g. Cerling, 1990).

2.3 Neotectonics of the Klamath Basin

The Klamath basin is bounded on either side by the East and West Klamath Lake fault zones, which are arrays of steeply dipping normal faults (Fig. 1). Onset of extension in the Klamath basin occurred as early as 7 Ma, and was ongoing by 4 Ma based on tilting of blocks on the east side of the basin associated with Basin and Range extension (Priest et al., 2013). The WKLFZ (Fig. 1) comprises a discontinuous series of north-northwest trending, predominately down-to-the-east normal faults. The fault zone is expressed at the surface as a series of fault scarps ranging from <1 – 30 m in height, offsetting glacial, glacio-fluvial, and debris-flow fan deposits preserved along the major drainages of the study area.

Historical, damaging earthquakes attest to the seismogenic potential of the faults in the Klamath Basin. Two M_w 6.0 earthquakes occurred along the Lake of the Woods fault in September of 1993, with epicenters just south of the study area (Fig. 1), causing an estimated $10 million in damage to the nearby city of Klamath Falls (Wiley et al., 1993). Notably, the earthquakes occurred without observed surface rupture (Wiley et al., 1993). The prominent fault scarps along the WKLFZ, formed during prehistoric surface-rupturing earthquakes, suggest the area has a history of even larger earthquakes (~M_w 7.0; e.g., Wells and Coppersmith, 1994).

In light of the recent earthquakes and the history of deformation implied by fault scarps, we seek to build on previous studies of Late Quaternary activity along the WKLFZ using new lidar and geochronology. Slip rates of ~0.2 mm/yr have been estimated previously based on the

offset glacial moraines in the study area (Hawkins et al., 1989). This value, however, is based on assumed ages of offset glacial deposits correlated to similar deposits in the Washington Cascades or the Sierra Nevada using relative weathering indices (e.g., boulder counts; Carver, 1972; Hawkins et al., 1989). Offset strata observed in seismic surveys of Upper Klamath Lake to the south of the study area yield rates varying from 0.14 mm/yr (Liberty et al., 2009) up to 0.43 mm/yr (Colman et al., 2000) for faults that offset lake sediments. K-Ar dating of offset lava flows west of Crater Lake ~ 20 km to the north of the study area, yielded slip rates of 0.3 – 0.35 mm/yr for the Annie Spring Fault (Fig. 1) (Bacon et al., 1997). These estimates are time-averaged over the entire WKLFZ, and therefore overlook the potentially spatially and temporally complex history of faulting suggested by mapping and interpretation of lidar data.

3. Surficial geologic mapping and lidar analysis

3.1 Mapping methodology and results

We use surficial geologic mapping and lidar analysis to identify and quantify offsets of datable landforms and surface deposits. Our mapping builds on previous work by Carver (1972) on the Mountain Lakes Wilderness to the south (Fig. 1), and mapping along the WKLFZ by Smith (1988). Dense forest cover hindered these previous mapping efforts, which predate lidar, now available via the Oregon Department of Geologic and Mineral Industries (http://www.oregongeology.org/lidar/). Using one-meter resolution bare-earth hillshade imagery derived from lidar we map glacial deposits (moraines, till, outwash), debris flow fans, stream terraces, and fault scarps along the length of the WKLFZ (Fig. 2). Mapping extends from the

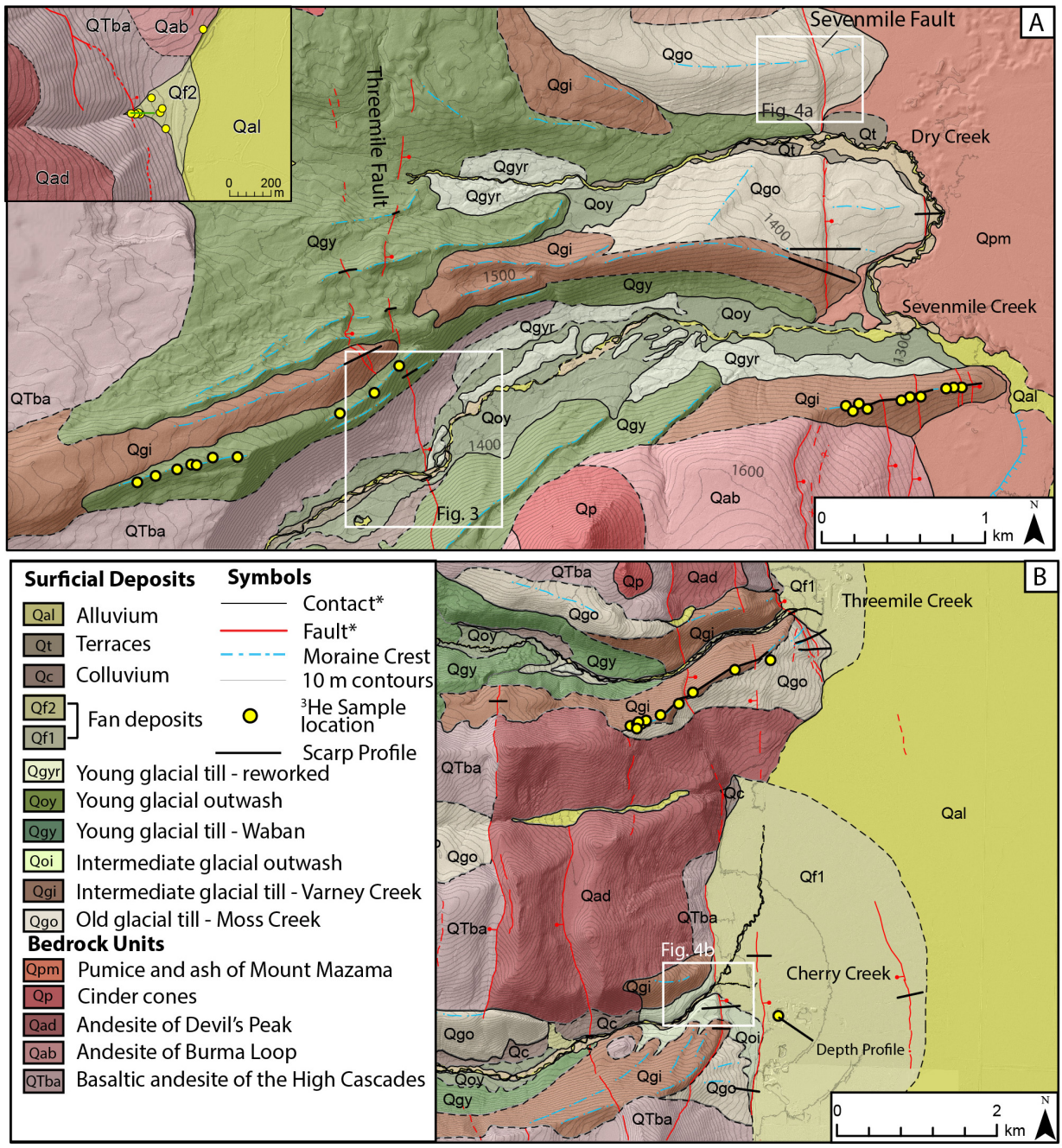

Figure 2. A) Surficial geologic map of Sevenmile and Dry Creeks over lidar bare earth hillshade available from the Oregon Department of Geology and Mineral Industries. Boxed areas shown in Fig. 3 and 4a. Inset - debris flow fan north of Threemile Creek. B) Surficial geologic map of Threemile and Cherry Creeks. Boxed area shown in Fig. 4b. Mapped creeks shown in figure 1. Bedrock mapping from Smith (1988). 3He sample data are reported in Table 2

range front in the east to the extent of the lidar near the heads of the glacial valleys in the west for a total mapped area of ~280 km^2 (Supplementary Fig. 1). Glacial deposits were differentiated

by relative age according to size, extent, degree of weathering (e.g., crest sharpness, dissection), relative position, surface morphology (e.g., kettle and kame topography or irregular hummocky surfaces adjacent to smooth deposits), and regional correlation to deposits mapped by Carver (1972) to the south. Qualitative observations of boulder frequency and weathering on the moraines corroborate the lidar-based mapping. Bedrock was mapped according to Smith (1982).

Mapping reveals at least three generations of glacial deposits (Qgo, Qgi, Qgy; Fig. 2) preserved along the lower extent of major drainages of the study area. We correlate the glacial deposits in the study area to the glacial deposits in the Mountain Lakes Wilderness (Carver, 1972) as follows: Qgo – Moss Creek Till, Qgi – Varney Creek Drift, Qgy – Waban Drift. Moss Creek deposits are preserved at the mouths of all major drainages (Fig. 2). They comprise large moraines that are significantly smoothed by post-deposition diffusion and often lack well-defined moraine crests. We observed a scarcity of boulders on these landforms. The few boulders present were heavily weathered. The tallest fault scarps observed along the WKLFZ, in some places exceeding 30 m height, cut these deposits along the range front at the mouth of each drainage.

Varney Creek (Qgi) deposits are partially, or in some cases completely, superimposed on Moss Creek deposits in all drainages except Rock Creek. This relationship is visible at Sevenmile Creek where a pair of large moraines are preserved extending out to the range front (Fig. 2a). The Varney Creek moraines are distinguished from older moraines by a lower degree of boulder weathering (Carver, 1972), and a better-defined morphology including relatively sharp moraine crests, such as observed on the southern side of the shared moraine between Sevenmile and Dry Creeks (Fig 2a). The large southern lateral moraine at Threemile Creek exhibits a similar relationship (Fig. 2b, supplementary Fig. 14 and 15). This moraine is

particularly important because we collected eleven cosmogenic exposure samples from boulders on its crest. The upvalley portion of the moraine crest is relatively sharp, consistent with other Varney Creek moraines. Rounded lateral and recessional moraine crests are preserved in the much more diffused portion of the moraine at the mouth of the valley, and appear to extend out from beneath the Varney Creek portion of the moraine. We delineate the smooth, diffused end of the moraine as the portion of the original Moss Creek moraine that was not resurfaced by the subsequent Varney Creek advance (see Supplementary Fig. 15 for uninterpreted lidar hillshade). Our field observations of boulder frequency support this interpretation. The Varney Creek portion of the moraine has a relative abundance of boulders relative to the Moss Creek portion, which is nearly devoid of boulders.

Waban stage deposits (Qgy) are preserved in all major drainages. Moraines are readily distinguished by their relatively small size and sharp crests inset within older moraines upvalley from the range front. The Waban is also characterized in places by kettle-kame topography, likely related to a period of ice stagnation during the retreat of Waban glaciers (Rosenbaum and Reynolds, 2004). Valley floors consist largely of outwash surfaces (Qoy) deposited during the retreat of Waban glaciers, grading down into large outwash fans (Qf1) built at the mouths of Threemile, Cherry, and Rock Creeks (Fig. 2b). Fans at the mouths of Dry and Sevenmile Creeks to the north are buried by ash fall deposits from Mt. Mazama (Fig. 2a).

We observe a number of post-glacial surfaces cut into or built on top of Waban outwash surfaces. We use the term "post-glacial" here to mean any deposit formed after the retreat of Waban glaciers. A series of fill terraces (Qt) are cut into Waban outwash surfaces and are preserved above the modern stream channels in each drainage (Fig. 3 and 4). Relatively steep (~5 – 15° slopes) debris flow fans (Qf2) are built up on top of glacial outwash fans in a number of

places (e.g., Fig. 2a inset). ~1 – 2 m fault scarps offset these young terrace or debris fan deposits in all five drainages.

Bedrock in the Sky Lakes Wilderness comprises three main volcanic units. The Andesite of Burma Loop and Klamath Point (Qab) (Fig. 2a) contains 15 – 25% phenocrysts of mostly subhedral, prismatic brown – black pyroxene with minor olivine, making it quite distinct in hand sample from the other two units. The Andesite of Devils Peak (Qad) (Fig. 2b) is characterized by vesicular boulders, with distinct clinkery aa textures. Black pyroxene phenocrysts make up <5% of the rock and the groundmass is aphanitic. These units overly the Basaltic Andesite of the High Cascades (QTba) (Fig. 2) which is an older series of undifferentiated flows (Smith, 1988).. It is blue-grey in color, with ~5% euhedral light green olivine being the only phenocryst present in most cases. Groundmass consists of a holocrystalline mesh of plagioclase, with small anhedral pyroxenes filling spaces in between grains.

We map numerous fault scarps that progressively offset multiple generations of glacial and post-glacial deposits across the ~ 10 km width of the WKLFZ (Figs. 1 and 2). Fault scarps indicate predominately steeply east dipping, N-NW trending faults that vary in length from ~5 – 15 km. Using moraine crests as piercing lines, we see no evidence for any lateral component of offset. Major faults include the Sevenmile, Threemile, and Cherry Creek faults (Fig. 1), named for the valley mouths cut by each fault (Bacon et al., 1997). Scarps are discontinuous, and made up of strands 1 – 5 km long. Small (~10 – 50 cm tall) fault scarps offset the basin floor outboard of the range front. We focus on faults offsetting all three generations of glacial deposits as well as post-glacial stream terraces and debris flow fans. These offset glacial and post-glacial deposits provided four generations of offset surfaces targeted for ^{3}He cosmogenic dating.

3.2 Scarp Profiles

We measure normal fault offset using topographic profiles across scarps extracted from lidar data (Table 1). Profiles are measured orthogonally across fault scarps where surfaces on both sides of the fault can reliably be matched. Vertical separation, dip-slip displacement, extension, and associated uncertainties are calculated using a Monte Carlo approach, following Thompson et al., (2002). This approach randomly draws from probability distribution functions for each input parameter for 100,000 trials to create a histogram of the predicted variable after a large number of trials and thus provide a measure of uncertainty. Here, we calculate offset from the geometry of linear regressions fit to the hanging wall, footwall and scarp face on a scarp profile, as well as the projection of the fault into the scarp face. The inputs therefore are the slopes and intercepts of the regressions, the dip and location of the fault, and uncertainties associated with each parameter. We determined fault dips based on local three-point problems using the lidar data allowing dips to vary ± 10° based on the distribution of dips measured (n=20) (Supplementary Fig. 13). Fault dips are generally steep, varying from ~70 – 85°, although a few faults appear to have gentler dips (~60°). The location where the fault plane intersects the fault scarp was allowed to vary between 1/3 and 2/3 of the scarp height (Thompson et al., 2002). This method is easily modified to include surface age as an input, allowing the calculation of rates of slip, vertical separation, and extension.

We measure profiles across fault scarps at 35 locations (Table 1; Supplementary fig. 1). Each profile is taken along an offset moraine crest, or an offset outwash or fan surface with known initial geometry. Dip-slip displacements of the three generations of glacial deposits span the following ranges: Moss Creek, ~4 – 40 m; Varney Creek, ~1 – 25 m; Waban, ~0.3 – 2 m. Post-glacial deposits are displaced between 0.5 – 3 m. In some cases individual fault strands that

Table 1 - Fault scarp profile data

Profile #	Latitude (DD)	Longitude (DD)	Age association (kyr)	Dip (°)[a]	Slip (m)[b]	Slip Rate (mm/yr)[b]
Dry Creek						
1	-122.0975	42.7404	168.9 ± 22.3	82	22.7 ± 1.6	0.13 +0.06/-0.02
2	-122.1310	42.7236	97.6 ± 12.7	60	9.5 +2.4/-2.8	0.09 +0.06/-0.04
3	-122.1290	42.7262	17.6 ± 2.1	82	1.3 ± 0.6	0.07 ± 0.04
4	-122.1322	42.7283	17.6 ± 2.1	78	0.8 ± 0.4	0.04 +0.04/-0.02
5	-122.1448	42.7375	17.6 ± 2.1	78	1.1 ± 0.4	0.06 ± 0.04
6	-122.1287	42.7315	17.6 ± 2.1	82	0.6 ± 0.2	0.04 ± 0.02
Sevenmile Creek						
7	-122.0889	42.7320	168.9 ± 22.3	80	7.5 ± 0.8	0.04 ± 0.02
8	-122.0966	42.7300	168.9 ± 22.3	86	18.6 +2.2/-1.6	0.11 +0.06/-0.02
9	-122.0922	42.7217	97.6 ± 12.7	80	5.5 +1.2/-0.8	0.06 +0.06/-0.02
10	-122.0896	42.7221	97.6 ± 12.7	86	4.2 ± 1.0	0.04 ± 0.02
11	-122.0860	42.7226	97.6 ± 12.7	55	1.3 ± 1.0	0.01 ± 0.02
12	-122.0968	42.7288	97.6 ± 12.7	86	17.9 +2.4/-2.0	0.18 +0.08/-0.04
13	-122.1274	42.7226	17.6 ± 2.1	82	1.6 ± 0.4	0.09 ± 0.04
14	-122.1260	42.7169	10.8 ± 1.6	82	1.3 ± 0.2	0.13 +0.10/-0.04
Threemile Creek						
15	-122.0789	42.6396	168.9 ± 22.3	80	24.6 ± 2.8/-3.6	0.14 +0.06/-0.04
16	-122.0795	42.6410	168.9 ± 22.3	80	41.9 +3.2/-2.8	0.24 +0.10/-0.06
17	-122.0885	42.6381	97.6 ± 12.7	75	7.6 ± 1.0	0.07 +0.04/-0.02
18	-122.0975	42.6345	97.6 ± 12.7	55	26.3 +3.8/-3.0	0.27 +0.14/-0.08
19	-122.1293	42.6327	97.6 ± 12.7	80	1.1 ± 0.2	0.01 ± 0.01
20	-122.0825	42.6439	20.4 ± 5.3	80	2.9 ± 0.4	0.12 +0.06/-0.02
21	-122.0854	42.6464	10.8 ± 1.6	80	1.7 +1.2/-1.0	0.16 ± 0.10
22	-122.0912	42.6626	10.8 ± 1.6	80	1.3 ± 0.4	0.12 +0.08/-0.04
Cherry Creek						
23	-122.0884	42.5875	168.9 ± 22.3	80	13.3 ± 1.9	0.07 +0.04/-0.02
24	-122.0927	42.5972	97.6 ± 12.7	78	21.5 +1.4/-0.6	0.12 +0.06/-0.02
25	-122.0926	42.5947	97.6 ± 12.7	78	18.5 +1.2/-0.8	0.18 +0.08/-0.04
26	-122.1136	42.5920	20.4 ± 5.3	65	1.2 ± 0.4	0.06 +0.08/-0.02
27	-122.0868	42.6033	20.4 ± 5.3	80	0.5 ± 0.1	0.03 ± 0.02
28	-122.0626	42.5991	20.4 ± 5.3	80	0.6 ± 0.1	0.03 +0.04/-0.02
29	-122.1136	42.5935	10.8 ± 1.6	65	1.5 ± 1.2	0.20 +0.1/-0.06
Rock Creek						
30	-122.1387	42.5659	168.9 ± 22.3	80	32.4 +2.2/-3.4	0.19 +0.08/-0.06
31	-122.1216	42.5618	168.9 ± 22.3	83	12.8 ± 0.8	0.07 +0.04/-0.02
32	-122.1171	42.5614	168.9 ± 22.3	83	4.2 +2.0/-1.2	0.02 ± 0.02
33	-122.0941	42.5484	20.4 ± 5.3	80	2.3 ± 0.8	0.10 +0.14/-0.06
34	-122.1624	42.5579	17.6 ± 2.1	80	0.3 ± 0.2	0.02 ± 0.02
35	-122.1099	42.5578	10.8 ± 1.6	85	0.8 ± 0.4	0.07 +0.06/-0.04

[a] Determined using three-point problems, or inferred from relation to topography
[b] Mode and 95% confidence interval reported

offset old deposits have smaller offsets than other fault strands that offset younger deposits. This indicates that some fault strands have been more active than others. The cumulative offset across the width fault zone of each successively older generation of deposit, however, exceeds that of the younger generations. Representative scarp profiles of each generation are shown in figures 3 and 4.

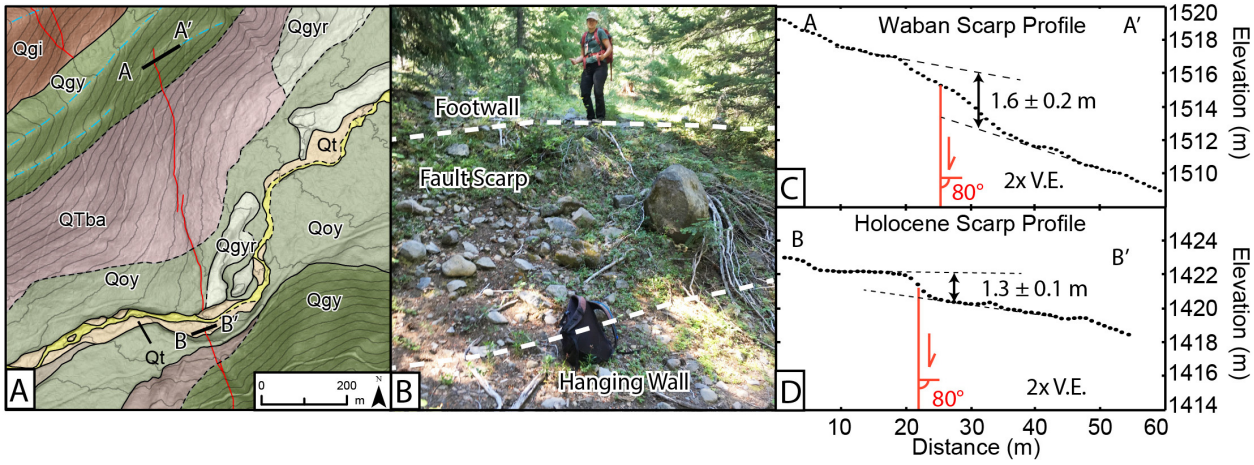

Figure 3. A) Map of offset Sevenmile Creek deposits. Mapped units are the same as Fig. 2: QTba - Basaltic andesite of the high Cascades; Qgi - Intermediate glacial till (Varney Creek); Qgy - Young glacial till (Waban); Qoy - Young glacial outwash; Qgyr - Young reworked glacial deposits; Qt - Terraces. B) Annotated field photo of fault scarp shown in panel D. C) Scarp profile of offset Waban moraine. D) Scarp profile of offset post-glacial terrace. Offsets reported are vertical separations. V.E. = vertical exaggeration.

Offset at Sevenmile Creek is concentrated on two main faults, each comprising multiple fault strands: the Sevenmile Fault which cuts the tips of the moraines at the mouth of the valley, and the Threemile Fault ~3 km up-valley (Fig. 2a). Large offsets occur along the Sevenmile Fault in Moss Creek and Varney Creek deposits. Moss Creek deposits have dip-slip displacements of up to ~23 m while Varney Creek deposits are offset by up to ~18 m. Threemile Fault offsets Waban stage moraines as well as post-glacial stream terraces on the valley floor by up to ~1.5 m (Fig. 3).

Offset at Threemile Creek is again concentrated on two main faults: the Threemile Fault at the range front and the Cherry Creek Fault ~1 km up-valley (Fig. 2b). Threemile Fault offsets Moss Creek moraines by up to 41.9 +3.2/-2.8 m. This fault also displaces a Waban outwash fan by 2.9 ± 0.4 m and a pair of Holocene debris flow fans by up to 1.7 +1.2/-1.0 m. Offset of a Varney Creek moraine occurs along two splays of the Cherry Creek Fault up valley, reaching up to 26.3 +3.8/-3.0 m.

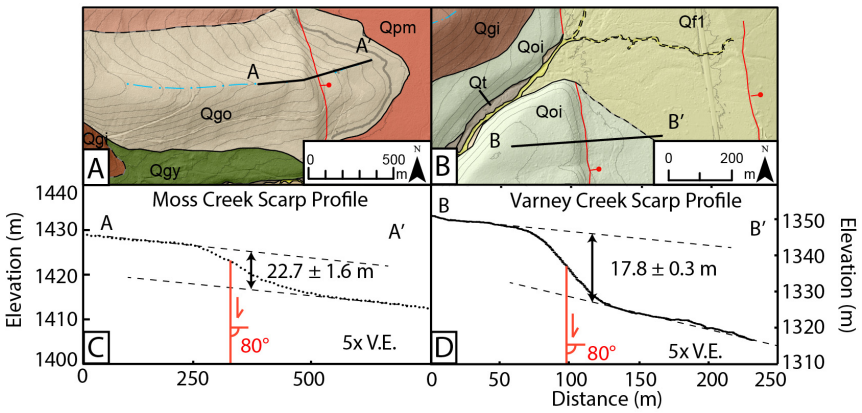

Figure 4. A) Map of an offset Moss Creek stage moraine at Sevenmile Creek. Location shown in Fig. 2a. B) Map of an offset Varney Creek stage glacial outwash terrace at Cherry Creek. Location shown in Fig. 2b. Mapped units are the same as Fig. 2: Qgo - Old glacial till (Moss Creek); Qoi - Intermediate glacial outwash (Varney Creek); Qgi - Intermediate glacial till (Varney Creek); Qf1 - Alluvial fan; Qt - Terraces. C) Scarp profile of offset Moss Creek stage moraine (Qgo) shown in A. D) Scarp profile of offset Varney Creek stage outwash terrace (Qoi) shown in B. Note the difference in scales between C and D. Offsets shown are vertical separation. V.E. = vertical exaggeration.

Offset at Cherry Creek is more distributed, occurring along the Cherry Creek Fault at the mouth of the valley, and several splays of more minor faults both inboard and outboard of the range front. Varney Creek stage outwash terraces are displaced by 21.5 +1.4/-0.6 m (Fig. 4) and a Varney Creek moraine is offset by 18.5 +1.2/-0.8 m. A Waban outwash fan extending from the mouth of the valley is offset in two places by 0.6 ± 0.1 m and 0.5 ± 0.1 m respectively. A Waban outwash surface is offset inboard of the range front as well, by 1.2 ± 0.4 m by a sharp, uphill facing, west dipping fault scarp. The same scarp displaces a post-glacial terrace on the other side of the valley by 1.5 ± 1.2 m.

Rock Creek does not contain any preserved Varney Creek deposits (Supplementary Figure 6). Moss Creek moraines are offset by as much as 32.4 +2.2/-3.4 m. A Waban outwash fan is displaced 2.3 ± 0.8 m at the mouth of the valley. The same small, uphill facing scarp that offsets Waban and post-glacial deposits in Cherry Creek extends continuously to the south across Rock Creek where it offsets a post-glacial terrace by 0.8 ± 0.4 m.

4. ^{3}He cosmogenic surface exposure dating

4.1 Boulder dating

Landform and surface ages rely on ^{3}He cosmogenic exposure dating of olivine and pyroxene rich boulders deposited on moraine crests and fan surfaces. We collected and analyzed 39 boulder samples from Moss Creek, Varney Creek, and Waban moraines, as well as a post-glacial debris flow fan (Table 2). We sampled large (> 1 m diameter), intact boulders, within 2 m of the crest in the case of the moraine samples (Supplementary Figs. 21 - 40). Samples were collected from the tops of boulders using a hammer and chisel to remove the outer few centimeters of intact weathering rind. Mineral separation to isolate pyroxene and olivine was conducted at Middlebury College. Samples were crushed and sieved to <300 μm, before being separated using standard heavy liquid techniques. Mineral separates were crushed before final loading in Tantalum packets for analysis.^{3}He/^{4}He isotope ratios were measured on a noble gas mass spectrometer at the Berkeley Geochronology Center. A description of the measurement process can be found in Blard et al. (2015). ^{3}He/^{4}He isotope ratios were calibrated using the CRONUS-P standard with a reported ^{3}He/^{4}He ratios of 102 ± 4 Ra (2σ) (Ra = 1.384 x 10^{-6}), with an overdispersion of 8.4% (2σ) (Blard et al., 2015).

Multiple production pathways for ^{3}He exist. Comparison of exposure samples to shielded samples – bedrock samples that have no prior exposure history – allows for the isolation of the cosmogenic component of ^{3}He used to calculate exposure ages (Amidon and Farley, 2011). Other production pathways of ^{3}He include nucleogenic ^{3}He produced through radiogenic neutron capture by ^{6}Li from the decay of U and Th, capture of muon-derived neutrons by ^{6}Li, and inherited ^{3}He from fluid inclusions from the magma chamber (Amidon and Farley, 2011). Shielded and exposure samples of a single unit are assumed to have homogenous composition

Table 2: Summary of ^{3}He Measurements

Sample Name	Unit	Latitude (DD)	Longitude (DD)	Elevation (m)	Thickness (cm)	Shielding Correction	Measured [^{3}He] (10^{6} atoms g^{-1})	Corrected [^{3}He] (10^{6} atoms g^{-1})[a]	Minimum exposure age (kyr)[b] erosion rate: 0 m/Myr	Maximum exposure age (kyr)[c] erosion rate: 3 m/Myr	Preferred exposure age (kyr)[d] erosion rate: 1 m/Myr
Shielded Samples											
KB16-02	Qad	42.6332	-122.0778	1273	---	---	2.1 ± 0.1	---	---	---	---
KB16-03	QTba	42.6661	-122.0871	1279	---	---	0.9 ± 0.0	---	---	---	---
KB16-05	Qab	42.6844	-122.0808	1279	---	---	1.6 ± 0.1	---	---	---	---
KB15-04	QTba	42.5924	-122.1082	1412	---	---	0.6 ± 0.0	---	---	---	---
Moss Creek / Varney Creek Composite Moraine											
KB16-01	Qad	42.6293	-122.1100	1711	4.0	0.996	35.4 ± 1.3	33.3 ± 1.3	73.5 ± 8.6	92.4 ± 13.9	78.6 ± 9.9
KB16-12	Qad	42.6299	-122.1077	1685	2.0	0.995	12.4 ± 1.0	10.3 ± 1.0	23.2 ± 3.5	24.6 ± 4.0	23.6 ± 3.7
KB16-13	Qad	42.6295	-122.1094	1697	3.0	0.997	54.7 ± 1.7	52.6 ± 1.8	114.1 ± 13.1	174.0 ± 32.8	126.7 ± 16.3
KB16-14	Qad	42.6294	-122.1100	1708	3.5	0.997	12.6 ± 0.8	10.5 ± 0.8	23.4 ± 3.2	24.9 ± 3.6	23.9 ± 3.3
KB16-15	Qad	42.6295	-122.1099	1706	3.0	0.996	46.1 ± 2.0	44. ± 2.0	95.9 ± 11.4	130.7 ± 22.4	104.3 ± 13.7
KB16-16	Qad	42.6293	-122.1102	1712	3.0	0.994	9.8 ± 0.7	7.7 ± 0.7	17.5 ± 2.7	18.2 ± 2.9	17.7 ± 2.7
KB16-17	Qad	42.6293	-122.1098	1704	3.0	0.991	42.0 ± 1.2	39.9 ± 1.3	87.6 ± 10.0	115.1 ± 18.1	94.7 ± 11.8
KB16-18	QTba	42.6333	-122.1002	1560	4.0	0.994	17.1 ± 0.8	16.3 ± 0.8	40.5 ± 4.8	45.3 ± 6.1	41.8 ± 5.2
KB16-19	QTba	42.6343	-122.0977	1535	3.5	0.996	9.4 ± 0.7	8.6 ± 0.7	22.2 ± 3.0	23.5 ± 3.4	22.6 ± 3.1
KB16-20	Qad	42.6366	-122.0934	1515	3.0	0.993	16.5 ± 0.8	14.4 ± 0.8	37.0 ± 4.6	40.8 ± 5.7	38.2 ± 4.9
KB16-21	Qad	42.6384	-122.0873	1447	3.5	0.992	57.2 ± 1.5	55.1 ± 1.6	145.8 ± 16.6	274.6 ± 69.9	168.9 ± 22.3
Varney Creek Moraine											
KB16-47	Qab	42.7210	-122.0962	1415	2.0	0.996	24.5 ± 0.9	22.9 ± 1.0	63.4 ± 7.5	76.7 ± 11.1	66.8 ± 8.4
KB16-48	QTba	42.7213	-122.0946	1406	2.0	0.996	21.9 ± 1.0	21.2 ± 1.0	59.1 ± 7.1	70.0 ± 10.1	62.2 ± 7.9
KB16-49	Qab	42.7213	-122.0944	1395	3.0	0.995	16.3 ± 0.9	14.7 ± 0.9	41.1 ± 5.2	46.3 ± 6.7	42.6 ± 5.6
KB16-50	Qab	42.7215	-122.0940	1396	2.0	0.997	6.9 ± 0.7	5.3 ± 0.8	15.5 ± 2.8	16.1 ± 3.0	15.7 ± 2.9
KB16-51	Qab	42.7217	-122.0919	1373	3.0	0.996	35.7 ± 1.5	34.1 ± 1.6	97.2 ± 11.6	133.6 ± 23.2	106.0 ± 13.9
KB16-52	Qab	42.7218	-122.0912	1384	3.0	0.996	32.2 ± 1.0	30.6 ± 1.1	86.9 ± 10.0	114.0 ± 18.0	94.0 ± 11.8
KB16-53	Qab	42.7221	-122.0903	1380	4.0	0.999	12.0 ± 0.7	10.4 ± 0.6	30.0 ± 3.9	32.8 ± 4.7	30.8 ± 4.1
KB16-54	Qab	42.7221	-122.0880	1360	4.0	0.997	32.4 ± 1.1	30.8 ± 1.9	89.9 ± 10.5	119.3 ± 19.3	97.4 ± 12.4
KB16-55	Qtba	42.7227	-122.0865	1357	4.0	0.997	12.9 ± 0.8	12.1 ± 0.9	35.7 ± 4.7	3943 ± 5.6	36.9 ± 5.0
KB16-56	Qab	42.7227	-122.0850	1338	3.0	0.996	30.8 ± 1.0	29.2 ± 1.1	86.3 ± 10.0	112.9 ± 17.9	93.3 ± 11.8
Waban Moraine											
KB16-04	Qab	42.7175	-122.1428	1733	3.0	0.996	8.1 ± 0.5	6.5 ± 0.6	14.9 ± 2.1	15.5 ± 2.3	15.1 ± 2.2
KB16-06	QTba	42.7160	-122.1499	1782	3.0	0.998	37.6 ± 1.6	36.9 ± 1.7	77.2 ± 9.0	98.1 ± 15.0	82.9 ± 10.4
KB16-07	Qab	42.7165	-122.1479	1762	3.5	0.998	7.5 ± 0.3	5.9 ± 0.4	13.0 ± 1.7	13.5 ± 1.8	13.2 ± 1.7
KB16-08	QTba	42.7169	-122.1456	1745	3.0	0.994	8.1 ± 0.4	7.3 ± 0.4	17.6 ± 2.0	18.4 ± 2.2	17.8 ± 2.1
KB16-09	Qab	42.7171	-122.1444	1744	4.0	0.996	8.6 ± 0.5	7.0 ± 0.6	15.7 ± 2.2	16.3 ± 2.4	15.9 ± 2.2
KB16-10	Qab	42.7173	-122.1442	1740	3.5	0.997	10.5 ± 0.6	8.9 ± 0.6	19.6 ± 2.7	20.6 ± 2.9	19.9 ± 2.7
KB16-11	QTba	42.7179	-122.1404	1717	3.0	0.998	7.7 ± 0.5	6.9 ± 0.5	17.2 ± 2.1	18.0 ± 2.3	17.5 ± 2.2
KB15-01	Qab	42.7214	-122.1303	1577	3.0	0.997	7.5 ± 0.1	5.9 ± 0.2	17.1 ± 1.9	17.8 ± 2.1	17.3 ± 1.9
KB15-02	Qab	42.7202	-122.1330	1618	3.0	0.997	9.7 ± 0.2	8.1 ± 0.2	19.6 ± 2.2	20.6 ± 2.5	19.9 ± 2.3
KB15-03	QTba	42.7240	-122.1274	1536	3.0	0.997	5.6 ± 0.1	4.9 ± 0.1	10.3 ± 1.2	10.5 ± 1.2	10.4 ± 1.2
Post-Glacial Debris Flow Fan											
KB16-23	QTba	42.6635	-122.0904	1284	3.0	0.977	3.7 ± 0.2	3.0 ± 0.5	5.5 ± 1.2	5.6 ± 1.2	5.5 ± 1.2
KB16-24	QTba	42.6628	-122.0910	1305	3.0	0.969	2.4 ± 0.1	1.7 ± 0.5	0.9 ± 0.6	0.9 ± 0.6	0.9 ± 0.6
KB16-25	QTba	42.6628	-122.0913	1305	4.0	0.966	3.6 ± 0.2	2.9 ± 0.7	11.1 ± 1.3	11.5 ± 1.3	11.2 ± 1.3
KB16-26	Qad	42.6627	-122.0911	1309	3.5	0.978	7.5 ± 0.7	5.4 ± 0.7	17.6 ± 3.1	18.4 ± 3.4	17.9 ± 3.2
KB16-27	QTba	42.6627	-122.0915	1313	3.5	0.958	3.4 ± 0.1	2.7 ± 0.7	10.5 ± 1.2	10.8 ± 1.3	10.6 ± 1.2
KB16-28	QTba	42.6627	-122.0899	1289	4.0	0.982	5.3 ± 0.3	4.6 ± 0.7	10.3 ± 2.0	10.6 ± 2.1	10.4 ± 2.0
KB16-29	Qad	42.6622	-122.0896	1281	2.0	0.973	4.3 ± 0.8	2.2 ± 0.9	7.2 ± 2.9	7.3 ± 3.0	7.2 ± 3.0
KB16-30	QTba	42.6629	-122.0897	1285	3.5	0.982	5.0 ± 0.9	4.3 ± 1.0	15.9 ± 3.2	16.6 ± 3.4	16.2 ± 3.2

[a] Measured ^{3}He concentration minus the shielded component of the corresponding unit (e.g. KB16-01 is from unit Qad so the corrected ^{3}He concentration is the measured ^{3}He for KB16-01 minus the measured ^{3}He concentration of KB16-02 - the shielded sample from unit Qad. For units with multiples shielded samples, the average ^{3}He concentrations is used)

[b-d] Exposure ages calculated using the CRONUS-Earth exposure age calculator (Balco et al., 2008) assuming a minimum erosion rate of 0 M/Myr, a maximum erosion rate of 3 M/Myr (Cerling et al., 1990), and a preferred erosion rate of 1 M/Myr based on observation of the sampled boulders

and have experienced the same formation and eruption history (and thus have the same ^{3}He concentration), with their paths diverging only when exposure samples were plucked by a glacier and deposited on a moraine. Thus, simply subtracting the measured ^{3}He concentration in a shielded sample from that of an exposure sample isolates the cosmogenic component of ^{3}He.

We collected shielded samples for each of three sampled units: the basaltic andesite of Klamath Point and Burma Loop (Qab), the basaltic andesite of Devils Peak (Qad), and the basaltic andesite of the High Cascades (QTba). These three units dominate the source area for moraine boulders (Fig. 2). Shielded samples for Qab and Qad were collected from road cuts at depths of 3.9 m and 5.3 m respectively, sufficiently below the attenuation depth from cosmogenic radiation. We collected two shielded samples for unit QTba, one from 3.9 m depth in a quarry, and the other from 8.0 m depth in a road cut. Their concentrations were averaged when subtracting from exposure samples (Table 2). The nucleogenic ^{3}He concentrations represent a relatively low percentage (~5 – 15%; Table 2) of the measured ^{3}He in the moraine exposure samples, which have been exposed long enough to accumulate relatively large amounts of cosmogenic ^{3}He. Samples from the post-glacial fan have a larger percentage of non-cosmogenic ^{3}He (up to 50%). High proportions of non-cosmogenic ^{3}He mean that it is more important to match each exposure sample with the correct shielded sample for more recently exposed samples. Individual boulder ages on the debris flow fan would be off by ~30-50% if paired with the incorrect shielded sample. The potential error on moraine samples is much lower, with individual ages varying only ~5-10%.

Surface exposure ages were calculated using the CRONUS-Earth online calculator, version 3, as described in Balco et al. (2008), using a time dependent production rate model and scaling scheme of Lifton et al. (2014). Because exposure age and erosion rate cannot both be

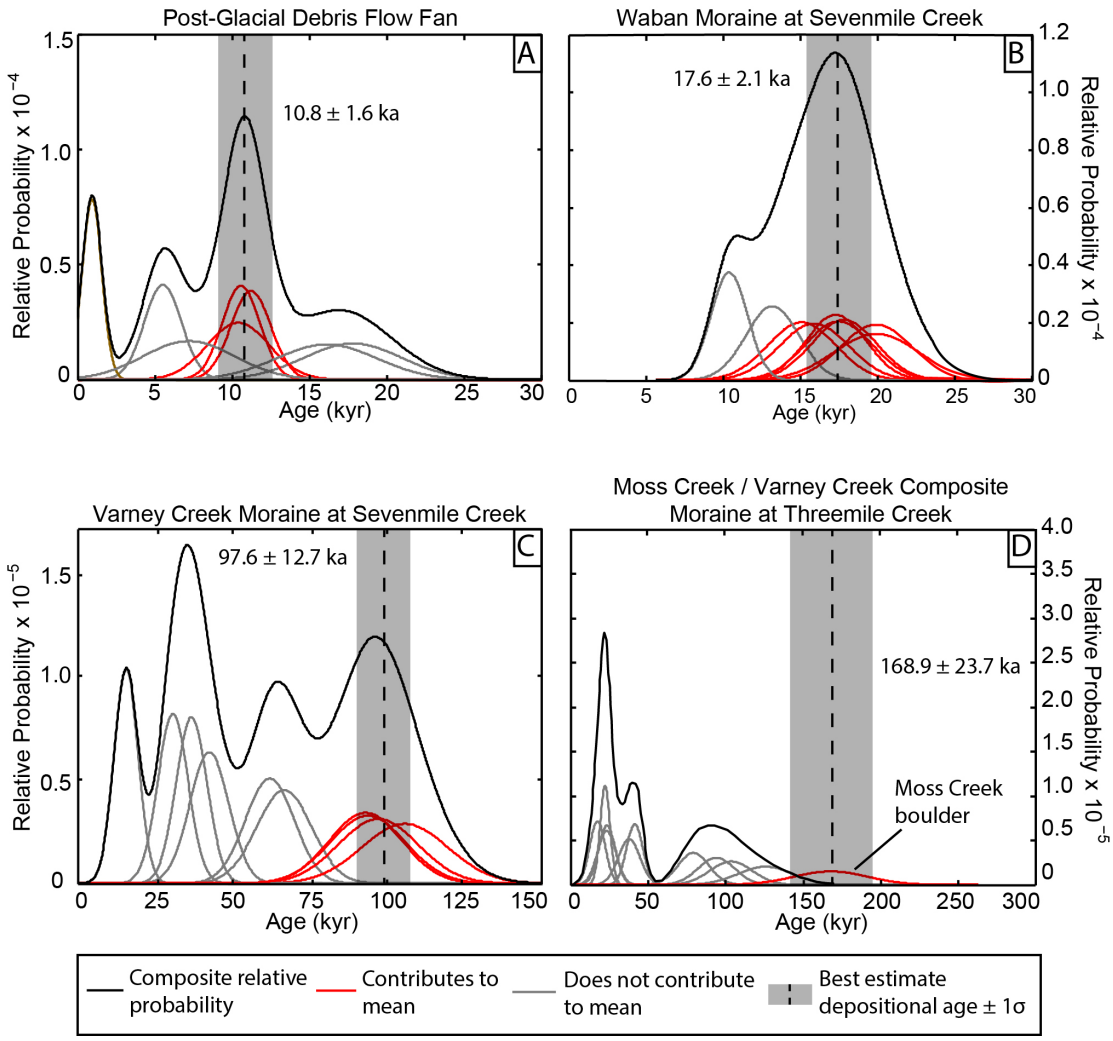

Figure 5. Probability density functions (PDFs) for four dated surfaces. Individual sample ages are defined by Gaussian PDFs shown in red and grey. Composite PDFs for the whole surface are shown in black. See Table 2 for individual sample data. See text for interpretation of data.

constrained using measurements of a single isotope, we calculate exposure ages using three erosion rate scenarios: 1) a minimum rate of 0 mm/yr (no boulder erosion); 2) a maximum rate of 3 mm/yr based on ^{3}He dating of basalt flows with ages previously constrained by K-Ar dating in Owens Valley, an area with comparable environmental conditions to the eastern Cascades (Cerling et al., 1990); 3) and an intermediate rate of 1 mm/yr based on studies of bare basalt bedrock weathering rates (Table 2; Bierman, 1994).

We use camel plots (Fig. 5), which plot individual sample ages and uncertainties (assuming 1 mm/yr boulder erosion) as Gaussian curves, to interpret a suite of samples as a

depositional age for a given surface. Pre- and post-depositional geologic processes result in spread in these distributions of ages. Boulder erosion and exhumation contribute to spread towards younger ages, while inheritance of previous exposure results in spread towards older ages. We look for peaks in the cumulative PDF resulting from clusters of individual samples to indicate the actual depositional age of a deposit. We compute a reduced χ^2 statistic (Table 3) for such peaks to test whether analytical uncertainty alone explains the scatter within the subgroup (Balco, 2011). From this we can estimate the probability that the age described by the peak in the cumulative PDF is significantly affected by the geologic processes described above.

The youngest dated surface is a debris flow fan north of Threemile Creek (Fig. 5a). Three samples contribute to a strong peak at 10.8 ± 1.6 ka (all reported age uncertainties are 1σ) using an assumed erosion rate of 1 mm/yr. One sample (KB16-24; Supplementary Figure 37) produces an anonymously low exposure age of 0.9 ± 0.6 ka. This young age may be attributed to post-depositional rolling of the boulder, or recent exhumation. We attribute the young ages (~5 ka and 7 ka) of samples KB16-23 and -29 to exhumation. We choose to exclude samples KB16- 26 and -30 from the calculation of the depositional age because they yield ages (~17 ka) consistent with the Waban Glaciation discussed below, however, mapping relationships indicate this fan post-dates the Waban. Inclusion of the other excluded samples does not shift the mean age of the surface, but does increase the uncertainty to ± 2.3 ka. We use the age 10.8 ± 1.6 ka as a rough estimate for the depositional age of all correlated post-glacial fans and terraces, acknowledging that the error is likely significantly larger than reported due to the potential range of depositional ages for these deposits. The broad application of the age of this fan age to all post-glacial surfaces has a minimal effect on calculated slip rates. The difference between the well

constrained age of the Waban and the ages of all post-glacial deposits is small relative to the difference in age between the Waban and the two older glacial periods.

We collected and analyzed ten samples from a Waban stage lateral moraine at Sevenmile Creek (Fig. 2a). One outlier (KB16-06) is excluded. We interpret this boulder to have been incorporated from the Varney Creek moraine just to the north of the sample location. The two youngest boulders are interpreted to be partially exhumed and excluded, leaving seven boulders to define an age of 17.6 ± 2.1 ka for the moraine. We apply this age to all Waban stage moraines. A second estimate of the timing of the Waban Glaciation is provided by a cosmogenic nuclide depth profile of a glacial outwash fan, detailed below.

Ten samples were collected from the Varney Creek moraine on the south side of Sevenmile Creek (Fig. 2a). Although the dates are scattered toward primarily younger ages, four samples cluster and produce a distinct peak at 97.6 ± 12.7 ka (Fig. 5c). We interpret this to represent the depositional age of the moraine. In this case, the boulders with younger exposure ages on the moraine have been exhumed. Other workers (e.g., Putkonen and Swanson, 2003) have observed that in data sets from older moraines, the effects of exhumation tend to dominate. In such cases, the oldest exposure age has been shown to be the most representative of the true depositional age of the deposit (Applegate et al., 2010; Applegate, 2012; Putkonen and Swanson, 2003). In this case, the oldest age is grouped in the cluster at ~98 ka.

We collected eleven samples from a composite Varney Creek and Moss Creek stage moraine at Threemile Creek (Fig. 2b). This interpretation is based on mapping and qualitative field observations of boulder frequency described in section 3.1. Ten of the eleven samples come from the Varney Creek portion of the moraine, while we only found one boulder on the Moss Creek portion of the moraine that met our sampling criteria. The Varney Creek ages are quite

Table 3 - Surface age summary

Mean Age (kyr)	n	Reduced χ^2 [a]	p [b]	Oldest Age (kyr)	Best estimate depositional age Age (kyr)
Post-glacial Debris Flow Fan					
10.8 ± 1.6	3	0.6	0.74	16.2 ± 3.2	10.8 ± 1.6[c]
Waban Moraine					
17.6 ± 2.1	9	7.8	0.45	82.8 ± 10.4	17.6 ± 2.1[c]
Varney Creek Moraine					
97.6 ± 12.7	4	9.0	0.1	106.0 ± 13.9	97.6 ± 12.7[c]
Moss Creek Moraine					
168.9 ± 22.3	1	---	---	168.9 ± 22.3	168.9 ± 22.3

[a]A statistical mesure of the scatter of ages from a surface

[b]The probability that scatter is from measurement uncertainty alone. A value <0.05 indicates that some geomporphic procees (e.g. exhumation, inheritance) may be respobinsible for some of the scatter

[c]Calculated after the removal of outliers

scattered, with a cluster of six anomalously young boulders grouped between 20 and 50 ka. The remaining four boulders have ages ranging from 78.6 ± 9.9 ka to 126.7 ± 16.3ka (Fig. 5d). Although these four ages are more scattered than those on the Varney Creek moraine at Sevenmile Creek, they are evenly distributed about a mean of ~ 100 ka, consistent with the estimated age of the Varney Creek advance. The Moss Creek boulder yields an age of 168.9 ± 22.3 ka. Although little confidence can be assigned to a single boulder age, we argue that this date at least provides an estimate for the age of the Moss Creek advance. The difference in moraine size and crest sharpness, the magnitude of offset relative to Varney Creek deposits, and the difference in boulder frequency and weathering all argue for this being an older advance, distinct from the Varney Creek. If the Oregon Cascades follow a pattern similar to other mountain ranges in the northern hemisphere, they experienced a major glacial advance associated with marine isotope stage six (~130 - 190 ka). Our date suggests that the Moss Creek deposits correspond to that period of glaciation. The timing of this advance in other ranges is not well constrained, due to similarly poor preservation of moraines and associated boulders. Estimates in the Sierra Nevada of California suggest an age of ~150 ka (Rood et al., 2011),

consistent with our date. We take 168.9 ± 22.3 ka to represent the approximate timing of the Moss Creek advance, however, because this date relies on a single boulder age on an evolving landform, the actual age uncertainty for this deposit is likely greater than the analytic uncertainty.

4.2 Depth profile

We collected a cosmogenic nuclide depth profile (Anderson et al., 1996) of six samples from the wall of a gravel quarry in the Waban outwash fan at the mouth of Cherry Creek (Fig. 6). Depth profiles rely on the fact that cosmic rays attenuate with depth below the surface. Thus, ^{3}He concentration decreases exponentially with depth. Because all clasts in an outwash fan have prior exposure obtained during transportation, all samples contain an inherited component of ^{3}He in addition to *in situ* the cosmogenic component. The relationship between ^{3}He concentration and depth is thus defined by the equation:

$$N(z) = N_o e^{-z/\lambda} + N_{inh} \quad (1)$$

where N(z) is the concentration of ^{3}He at a depth, z, N_o is the concentration at the surface, λ is the attenuation length for production by high-energy spallation, and N_{inh} is the inherited component of ^{3}He.

We collected samples every 15 cm between depths of 45 and 110 cm, and a sixth sample at 150 cm depth. We sampled a mixture of sand and gravel clasts, which were prepared and analyzed following the same procedure as the boulder samples. Because lithology could not be determined for individual clasts, we apply no shielded sample correction to the measured ^{3}He concentrations. The observed pattern of exponentially decreasing ^{3}He concentrations supports the assumption that the sampled upper surface of the fan was deposited rapidly. This pattern also supports the assumption that the ^{3}He measured is cosmogenic, not produced through another

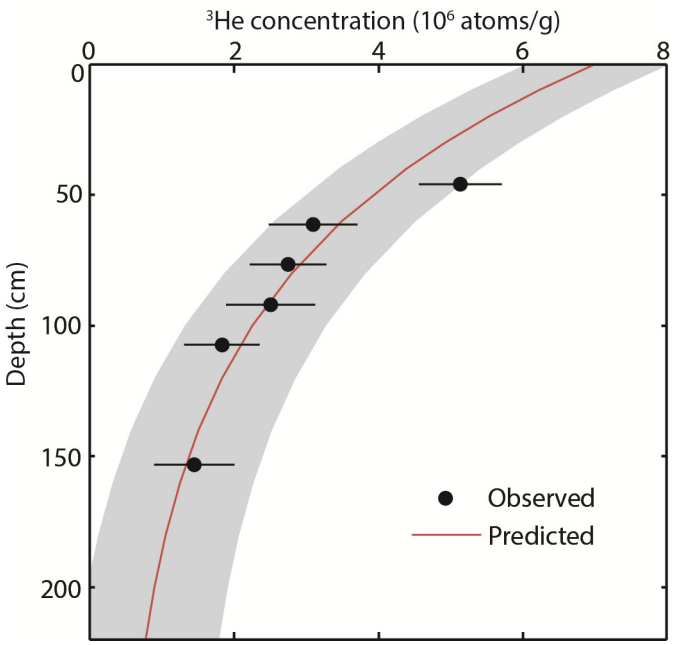

Figure 6. Cosmogenic 3He depth profile from the Waban glacial outwash fan at the mouth of Cherry Creek. Grey band is 1σ uncertainty based on measured uncertainty of samples. The modeled surface concentration yields a depositional age of 20.4 ± 5.3 ka.

pathway discussed above. We fit equation 1 to the data by minimizing the sum of the squares of the errors between the measured ^{3}He concentrations and values predicted by the function (Fig. 6). The best-fit result was then solved for the surface concentration, which was in turn used to calculate the age of the surface using the CRONUS-Earth calculator. Using a value of 160 g/cm^3 for λ (Gosse and Phillips, 2001), and a density of 2 g/cm^3, the best fit-model yields a modeled inherited component of 0.35 x 10^6 ^{3}He atoms/g and a modeled surface concentration of 6.7 ± 1.6 x 10^6 ^{3}He atoms/g (1σ uncertainty reflecting uncertainties in measured samples. This surface concentration corresponds to an age of 20.4 ± 5.3 ka, which we apply to Waban outwash surfaces in the area.

5. Fault slip rates

5.1 Extension Rate Transects

Surface age constraints combined with offset measurements provide a late-Pleistocene record of fault slip rate along the WKLFZ. We consider both the extension rate and dip-slip rate across the entire fault zone. Because the faults are all north striking, we compare their E-W

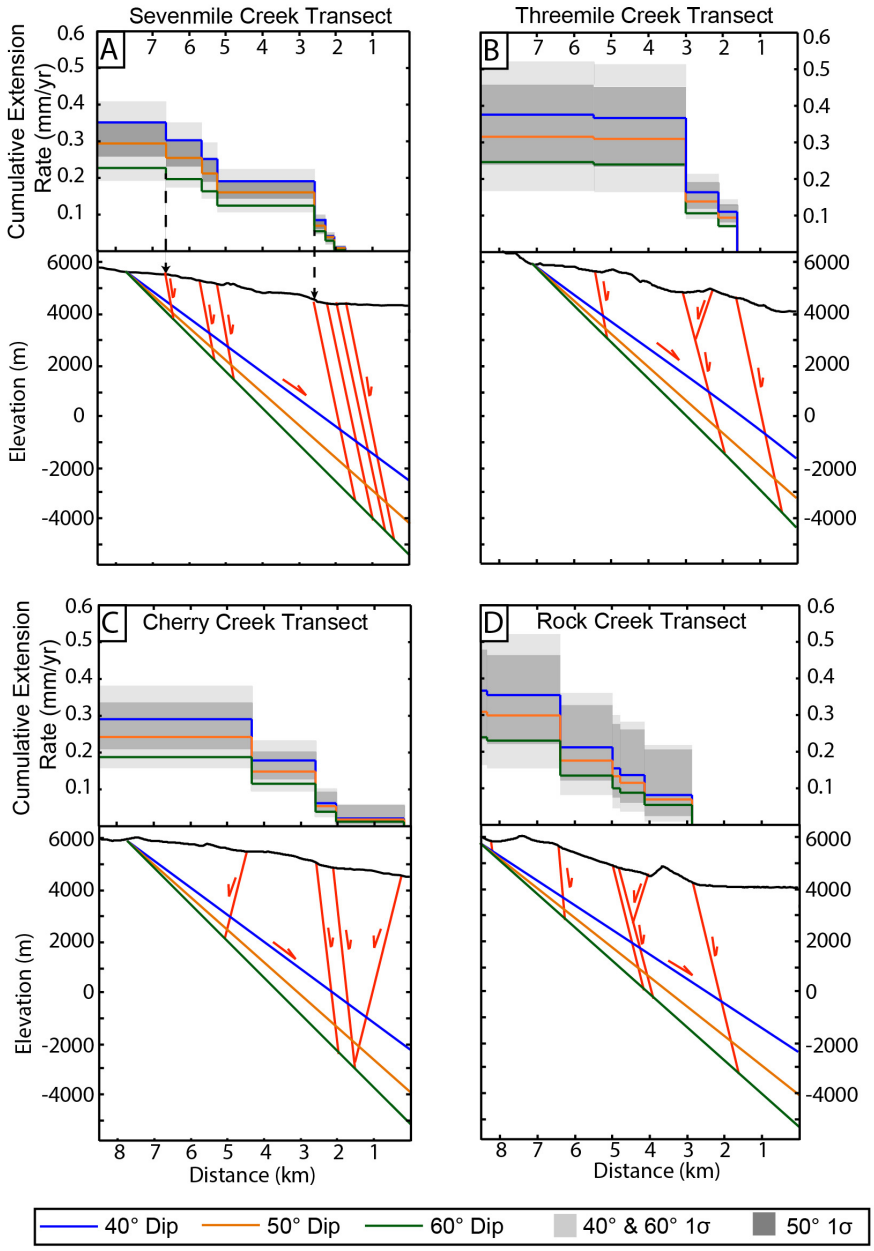

Figure 7. Transects across the WKLFZ along four main drainages in the study area (Fig. 2, 3). The transect down Sevenmile Creek includes the Dry Creek offsets. Extension rate reported is the extension rate on a master fault at depth due to the cumulative offset on many steep surficial faults across the width of the fault zone. Rates are summed from the range front on the right (east) to the western edge of the fault zone on the left. Jumps in cumulative extension rate correspond to the steep surficial faults shown directly below. Faults shown in cross section are schematic.

oriented extension rates to the E-W components of GPS-based horizontal surface velocities (McCaffrey et al., 2013) to understand the WKLFZ's role in accommodating the extension of the basin. We measure four transects across the fault zone (Fig. 7), summing the extension rate on each fault to determine the cumulative extension rate across the WKLFZ. Transects were constructed by projecting offsets on either side of a drainage onto an E-W profile down the valley axis. We constructed these for four of the five major drainages. Offsets from the northernmost drainage (Dry Creek) were included in the Sevenmile transect due their proximity and the fact that they share a medial moraine. Extension rates were calculated using the Monte Carlo approach outlined in section 3.1. We choose to average extension rates

over the entire time range spanned by dated deposits, rather than considering potential rate changes with time. While the fault zone as a whole may exhibit a rate change, we cannot determine how or if rates changed on the individual fault splays considered in the extension rate transects.

Measured three-point problems (Supplementary Fig. 13) only constrain fault dips at the surface. No constraints exist for the dip of faults at depth, though they likely merge into a single master fault (Bacon et al., 1997). Focal mechanisms from the 1993 earthquakes indicate the that the Lake of the Woods fault to the west (Fig. 1) has a dip of ~50° east at a depth of ~10 km (Braunmiller et al., 1995; Dreger et al., 1995). Assuming a similar dip for the WKLFZ the extension rate on the master fault at depth will be higher than that indicated by the steeply dipping surface faults. Figure 7 presents extension rates on the master fault for a range of fault dips. Extension is split up relatively evenly on four to seven faults in each drainage. Average extension rates across the entire fault zone are 0.3 ± 0.2/-0.1 mm/yr (95% confidence interval) for a 50° dipping master fault (Fig. 7).

5.2 Fault slip rates through time

We obtain a simple measurement of slip rate across the WKLFZ by normalizing dip slip measurements by the age of the associated offset deposit. We consider the cumulative slip across the fault zone for each of the four dated generations of deposits. We sum slip across each of the four transects shown in Figure 7 to account for along strike variations in slip. Fitting a regression to those data yields slip rates of ~0.2 – 0.3 mm/yr averaged over the time interval spanned by

dated deposits (Fig. 8). This analysis serves as a baseline estimate of slip rate, but ignores any potentially temporally complex pattern of faulting.

In an attempt to capture this complexity, we calculate fault slip rates using a python-based slip rate calculator, available for download online at https://github.com/cossatot/slip_rate_calculator (Styron, 2015). The calculator uses a Monte Carlo approach to calculate slip rates and assess the likelihood that slip rate has changed on a given fault over the time interval spanned by offset markers. The calculator randomly draws from input probability distribution functions (PDFs) for the age and offset of each marker, fitting a single regression to the data in the case of a constant slip rate, or two regressions separated by an inflection point in the case of a change in slip rate. This process is repeated for the desired number of iterations (10,000 in this case) to produce a distribution of slip rate(s).

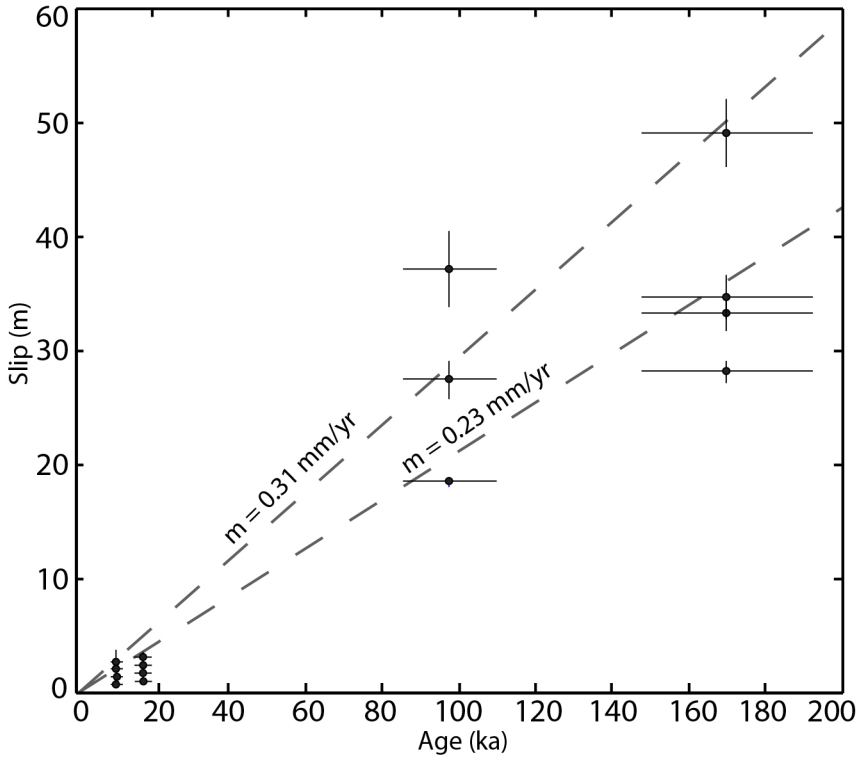

Figure 8. Slip as a function of age of an offset marker. Slip on each generation of deposit is summed across the fault zone for each of the transects shown in figure 7. Each data point represents the cumulative offset across the fault zone of a given generation of deposit for a given transect. Error bars are 1σ. Bottom dashed line is linear regression fit to all data. Top dashed line is linear regression fit to maximum offsets for each age of marker, representing a maximum possible slip rate. The slopes of the regressions represent slip rates.

This method has several advantages over other

methods of detecting changes in slip rates through time. First, it allows the inputs of offset and surface age to be custom PDFs, in the case where one or both are not well described by typical Gaussian distributions. Second, it does not require that a potential change in slip rate coincide with the age of an offset marker (e.g., Gold and Cowgill, 2011). Rather, any inflection point – the point at which the change in slip rate occurs – is determined by randomly sampling a number of potential inflection points for each iteration. A piecewise fit is then performed for each potential inflection point, and the best least-squares fit for that iteration's sampled marker values is the output result. The slopes of the two regressions represent two different slip rates, with the inflection point representing the timing of the change in slip rate. A sufficiently large number of iterations produces distributions for the inflection point and both slip rates. Finally, the calculator does not assume *a priori* that a change in slip rate has occurred. Rather, it assesses the likelihood that a change in slip rate has occurred by testing two models: one in which a single, constant slip rate is fit to the data, and another where an inflection point is determined and two slip rates are fit. These models are compared using a statistical test based on the Bayesian Information Criterion, which rewards models for goodness of fit, but penalizes them for complexity. It then reports the proportion of trials that produced slip-rate-change models that fit the data better than constant-slip-rate models (or vice versa).

For the WKLFZ as a whole, slip magnitude for each generation of offset marker was summed across transects shown in Figure 7 as described above. The cumulative slip for each age was then averaged over the four transects, producing the average north-south cumulative slip for each generation of deposit across the entire WKLFZ. We calculate slip rates by combining these average offsets with the ages of offset markers in the slip rate calculator discussed above. Slip rate increases from 0.06 +0.08/-0.05 mm/yr (mode and 95% confidence interval) to 0.27 +0.1/-

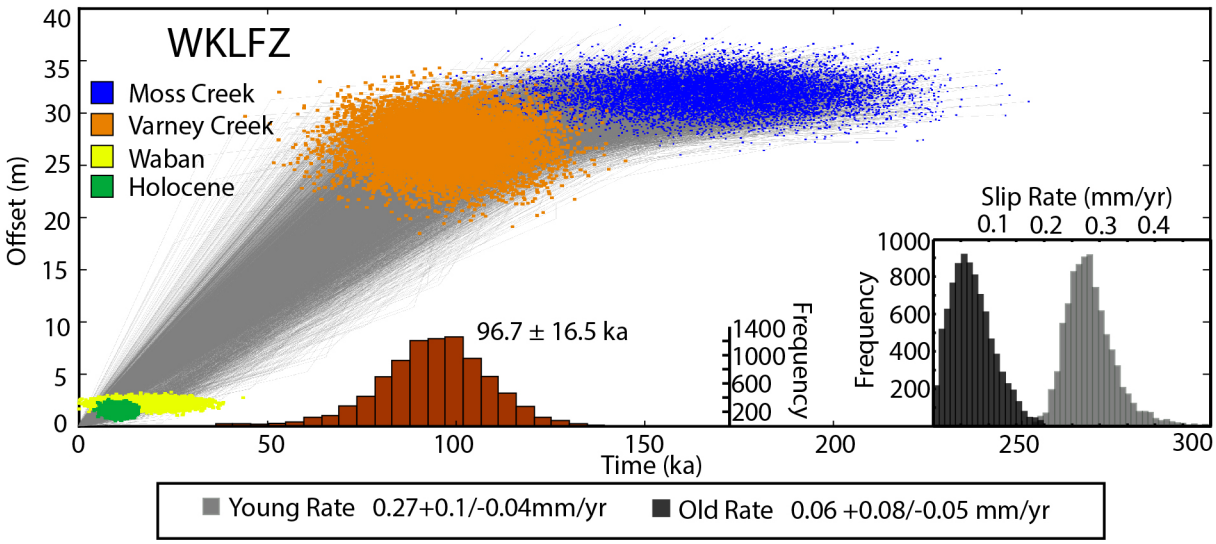

Figure 9. Monte Carlo simulation results for slip rates across the entire WKLFZ. Distributions correspond to inputs for each four generations of offset marker drawn from probability distribution functions defined by the mean offset and surface age and associated uncertainties. Gray lines are the best fit linear or piece-wise functions for individual iterations. Histogram showing the output distribution for the timing of rate change (mean and 1σ uncertainties reported) is shown in red along the x-axis. A histogram showing the output distributions for old slip rates (prior to the rate change) and young slip rates (after the rate change) is shown in the lower right corner. Slip rates reported as mode and 95% confidence interval.

0.04 mm/yr (Fig. 9). The change in slip rate occurs at 96.7 ± 16.5 ka (1σ). A piecewise fit – indicating a change in slip rate – is the more appropriate model in 83% of the 10,000 iterations. This analysis was also performed using every individual offset marker as inputs, rather than the average slip along the entire length of the fault. It produces the same pattern of slip rates increasing from ~0.05 – 0.3 mm/yr, though with larger uncertainties due to the large range of offsets of older deposits by individual fault strands.

6. Discussion

6.1 Glacial chronology of the Klamath Basin

Thirty-nine new cosmogenic ^{3}He surface exposure dates and a cosmogenic nuclide depth profile constrain the glacial chronology of the Klamath Basin. The age of the Moss Creek stage

is underconstrained. It relies on a single boulder dated at 168.9 ± 22.3 ka. We assign little confidence to this exact age, however we find it useful as an estimate. It overlaps with measurements of the correlative Tahoe stage in the Sierra Nevada at 144 ± 7 ka (Rood et al., 2011). The Moss Creek – Varney Creek interval slip rates (Fig. 9) are similarly underconstrained as they rely on the age of the Moss Creek. The overall pattern of quickening slip rates, however, holds for any age of the Moss Creek older than ~120 ka. An age younger than this produces a Moss Creek – Varney Creek interval slip rate in line with post-Varney Creek slip rates, while an age older than this produces slip rates slower than post-Varney Creek rates. 120 ka is younger than both our estimate for the Moss Creek and estimates for the Tahoe of the Sierra Nevada, and only ~20 kyr older than our measured age of the Varney Creek stage. While we cannot definitively say the Moss Creek is older than 120 ka, the round, diffuse shape of the Moss Creek moraines, and higher fault offsets and lower boulder frequency relative to Varney Creek deposits, provide additional evidence that the Moss Creek may be substantially older than the Varney Creek. If this is the case then slip rates on the WKLFZ have increased since ~100 ka.

Our age of 97.6 ± 12.7 ka for the Varney Creek Glaciation is supported by the other sequence of dated moraines in the Cascades. Swanson and Porter (2008) obtained ages of moraines near Leavenworth, WA, the only other cosmogenically dated sequence of moraines in the Cascades, using ^{36}Cl dating. These ages, however, were calculated using now outdated production rates, which may result in younger apparent ages. They note two advances – the pre-Mountain Home and the Peshastin – at 93.1 ± 2.6 ka and 105.4 ± 2.2 ka (1σ analytical uncertainty). Our estimate of 97.6 ± 12.7 ka for the Varney Creek could correlate to either of the pre-Mountain Home or the Peshastin of the Washington Cascades. Lava – ice contact structures have been observed in lava flows in several of the glacial valleys surrounding present day Crater

Lake, some correlated to marine isotope stage 5d (~100 ka) (Bacon and Lanphere, 2006). This observation suggests that there were glaciers present in the region during this time period.

We recognize that ~98 ka is an uncommon age for glacial deposits in North American mountain ranges. We therefore consider alternative explanations for this age besides a major glaciation at this time, and what implications they could have on our measurement of slip rates. The fact that clusters of boulders around this age are present on moraines at both Threemile and Sevenmile Creek suggests that there was some common process at work in both valleys. Exhumation appears to be an important process on these moraines, based on the presence of numerous anomalously young boulders on the two older dated moraines. It is possible that these moraines are older than the boulder exposure ages indicate, and all of the samples have been at least partially exhumed. An older surface would result in lower slip rates since the Varney Creek, bringing rates closer to pre-Varney Creek slip rates, and reducing or eliminating the apparent change in slip rates.

The Cascades of Washington show two younger advances – the Leavenworth II and the Leavenworth I – at 16.1 ± 1.1 ka and 19.1 ± 3.0 ka respectively (Swanson and Porter, 2008). These dates broadly correlate to our date of 17.6 ± 2.1 ka for the Waban moraine at Sevenmile Creek. ^{10}Be dating of a moraine sequence in the Wallowa Mountains give similar dates of 17.0 ± 0.3 ka and 21.1 ± 0.4 ka associated with last glacial maximum. Our date is also in agreement with the date of Tioga stage moraines in the Sierra Nevada at 18.8 ± 1.0 ka (Rood et al., 2011). Lake cores from Upper Klamath Lake provide an estimate of ~18 – 19 ka for last glacial maximum in the Klamath Basin (Colman et al., 2004), also in good agreement with our measurements. The age of the Waban outwash fan at the mouth of Cherry Creek is slightly older

than the age suggested by the moraine at Sevenmile Creek. This older date aligns with the older last glacial maximum advance observed in the Wallowas: 21.1 ± 0.4 ka (Licciardi et al., 2004).

Based on the dates discussed above, we alter Carver's (1972) correlations to the Sierra Nevada of California. We correlate the Moss Creek to the Tahoe instead of the Mono Basin. The Waban is still correlated to the Tioga, and the Varney Creek represents an intermediate advance that may not have occurred in the Sierra Nevada.

6.2 Implications of extension rates on basin structure

Despite the complex pattern of faulting exhibited by the surface trace of the WKLFZ, the cumulative offset across the fault zone is remarkably similar along strike. For a given master fault dip, the cumulative extension rate across the fault zone is almost identical for each of the four transects shown in figure 7. This supports the hypothesis that the complex surface expression of offset is controlled by slip on a single fault at depth (Bacon et al., 1997). A 50° dip of the WKLFZ at depth produces extension rates of ~ 0.3 mm/yr across the fault zone. Geodetic data in the area are sparse, but GPS stations on either side of the basin allow comparison of our measured extension rate with rates inferred from modern geodesy. We use the relative difference in E-W horizontal surface velocities (Fig. 1; McCaffrey et al., 2013) of these stations to estimate the modern extension rate of the basin. Although the uncertainties on the velocities are high enough that they overlap, comparison of the average velocities yields extension rates of 0.3 – 0.9 mm/yr. This indicates that the WKLFZ accommodates a significant portion of the modern-day extension of the basin, with the remainder potentially taken up on the East Klamath Lake Fault Zone and the Lake of the Woods Fault Zone (fig 1).

6.3 Temporal changes in fault slip rate on the WLKFZ

Our results indicate that there may have been a distinct increase in slip rate for the WKLFZ at ~100 ka (Fig. 9).The magnitude of the rate change is dependent on the underconstrained age of the Moss Creek moraines, although the overall pattern of increasing slip rates holds for any age older than ~120 ka.

We can only speculate on potential drivers of a change in slip rate during this interval, though volcanic activity surrounding Mt. Mazama may play a role. Extensive study of the eruptive history of Mt. Mazama reveals a change in both the regional and local Mazama activity between ~120 and 80 ka (Bacon and Lanphere, 2006). Active regional volcanism between ~160 and 120 ka preceded concentration of volcanic activity around Mt. Mazama at ~80 ka, leading up to the climactic eruption ~7700 kyr ago. Increases in tectonic activity associated with volcanic activity have been observed near volcanic centers in Italy (Cosncetta et al., 1998), Hawaii (Troise, 2001; Walter and Amelung, 2004); associated with the Long Valley Caldera in eastern California (Bursik et al., 2003); in Kamchatka (Walter, 2007); and in the Yellowstone – Teton region of Wyoming (Hampel and Hetzel, 2008). We note that the shift from distributed regional volcanism to concentrated activity around Mt. Mazama between ~120 and 80 ka encompasses the timing of the change in slip rate at ~100 ka.

An increase in slip rates induced by glacial unloading (e.g. Hetzel and Hampel, 2005; Hampel and Hetzel, 2007) following the recession of the Varney Creek glaciers is another possibility. This hypothesis, however, raises the question of why such a change is only observed following one of the three major glacial advances observed in the area.

Our slip rate estimates broadly agree with previous measurements of slip rate in nearby areas, accounting for prior work lacking the temporal resolution to detect variations in slip rate. A slip rate of 0.3 mm/yr over the past 300 kyr is estimated from offset lava flows (dated by K-Ar) west of Crater Lake, and due north of our study area (Bacon et al., 1999). This longer-term rate is in agreement with our measurement of 0.27 +0.10/-0.04 mm/yr since the Varney Creek Glaciation on the WKLFZ. This agreement suggests that the increase in slip rates we observe may actually be a return to the long-term average rate, with the low rates following the Moss Creek Glaciation being the deviation. The seismic reflection data of Colman et al., (2000) indicate a post-Mazama slip rate of 0.43 mm/yr, exceeding both our own and others' estimates for the long-term slip rate in the area. Liberty et al., (2009) also performed seismic reflection surveys across Klamath Lake, finding vertical slip rates ranging from 0.14 – 0.25 mm/yr, consistent with previous estimates. They argue that the use of the Mazama tephra as an offset marker may not produce slip rates that are representative of the long-term average, given the relatively long recurrence interval between large earthquakes.

Although the timing of any earthquakes outside of the 1993 events is unknown, the difference in offset between Waban stage and Holocene deposits allows us to speculate on the recurrence interval of earthquakes along the WKLFZ, at least since last glacial maximum. The average offset of Holocene deposits is 1.5 m, while the average offset of Waban deposits is 2.2 m. This difference in offset may only represent one or two earthquakes (assuming ~0.5 – 1 m of offset per surface rupturing earthquake). That suggests that the recurrence interval for large, surface-rupturing earthquakes may be on the order of the interval period between the dated Waban and post-glacial deposits, ~ 5 – 10 kyr. This is in agreement with previous estimates of recurrence intervals of 3 – 7 kyr for M_w 7 earthquakes in the region (Bacon et al., 1999).

Observed offsets of up to 3.1 m of Mazama tephra in seismic-reflection profiles of Upper Klamath Lake suggest a much higher recurrence interval, with as many as three large earthquakes occurring in the last 7 kyr (Colman et al., 2000).

7. Conclusion

The combined results of new geochronologic and lidar measurements yield insights into the late-Pleistocene glacial and tectonic history of the West Klamath Lake Fault Zone in southern Oregon. We show that ^{3}He cosmogenic exposure dating is a viable dating method for deposits in the region. Forty-five new ^{3}He cosmogenic exposure dates provide only the second geochronologically constrained glacial sequence in the Cascade Range, and the first in the Cascades of Oregon. We date the two most recent major glacial advances in the area at 97.6 ± 12.7 ka and 17.6 ± 2.1 ka. The latter date is in line with previous estimates of the last glacial maximum in the region. These dates are in agreement with moraines dated in the Cascades of Washington, the Wallowas of northeast Oregon, and the Sierra Nevada of California. We also provide an estimate for the timing of an older glacial advance at 168.9 ± 22.3 ka, which may correlate to the Tahoe advance of the Sierra Nevada. Additionally, we date a post-glacial debris flow fan at 10.8 ± 1.6 ka.

Combined with lidar-based surficial geologic mapping and fault scarp measurements, the new dates allow the detailed reconstruction of fault slip rates on the WKLFZ. We calculate average slip rates of ~0.2 – 0.3 mm/yr over the last ~170 kyr, in agreement with previous measurements of slip rate in the area. Extension rates across the fault zone are constant along the

north-south length of the zone, consistent with a fault zone that merges to a single master fault at depth.

We use a python-based slip rate calculator with a Monte Carlo approach to detect and quantify the likelihood of a change in slip rate over the time range spanned by dated deposits. This approach reveals there may have been an increase of slip rates across the fault zone at 96.7 ± 16.5 ka, from 0.06 +0.08/-0.05 mm/yr to 0.27 +0.1/-0.04 mm/yr (mode and 95% confidence interval). These calculations rely on the estimated age and correlation of the oldest glacial deposits in the area, which carries significant uncertainty. Considering just the time interval since the oldest well constrained glaciation at ~98 ka, measured slip rates are constant at ~ 0.3 mm/yr across the fault zone, in good agreement with prior measurements in the area.

References

Amidon, W.H. and Farley, K.A., 2011. Cosmogenic 3 He production rates in apatite, zircon and pyroxene inferred from Bonneville flood erosional surfaces. Quaternary Geochronology, 6(1), pp.10-21.

Anderson, R.S., Repka, J.L., Dick, G.S., 1996. Explicit treatment of inheritance in dating depositional surfaces using in situ ^{10}Be and ^{26}Al: Geology v. 24 (1), p. 47–51.

Amos, C.B., Brownlee, S.J., Rood, D.H., Fisher, G.B., Bürgmann, R., Renne, P.R. and Jayko, A.S., 2013. Chronology of tectonic, geomorphic, and volcanic interactions and the tempo of fault slip near Little Lake, California. Geological Society of America Bulletin, 125(7-8), pp.1187-1202.

Applegate, P.J., Urban, N.M., Laabs, B.J.C., Keller, K. and Alley, R.B., 2010. Modeling the statistical distributions of cosmogenic exposure dates from moraines. Geoscientific Model Development, 3(1), p.293.

Applegate, P.J., Urban, N.M., Keller, K., Lowell, T.V., Laabs, B.J., Kelly, M.A. and Alley, R.B., 2012. Improved moraine age interpretations through explicit matching of geomorphic process models to cosmogenic nuclide measurements from single landforms. Quaternary Research, 77(2), pp.293-304.

Bacon, C.R., 1983. Eruptive history of Mount Mazama and Crater Lake caldera, Cascade Range, USA. *Journal of Volcanology and Geothermal Research*, *18*(1-4), pp.57-115.

Bacon, C.R., Gunn, S.H., Lanphere, M.A. and Wooden, J.L., 1994. Multiple isotopic components in Quaternary volcanic rocks of the Cascade arc near Crater Lake, Oregon. Journal of Petrology, 35(6), pp.1521-1556.

Bacon, C.R., Mastin, L., Scott, K. and Nathenson, M., 1997. Volcano and earthquake hazards in the Crater Lake region, Oregon. US Geological Survey Open-File Report, 97(487), p.32.

Bacon, C.R., Lanphere, M.A. and Champion, D.E., 1999. Late Quaternary slip rate and seismic hazards of the West Klamath Lake fault zone near Crater Lake, Oregon Cascades. *Geology*, *27*(1), pp.43-46.

Bacon, C.R. and Lanphere, M.A., 2006. Eruptive history and geochronology of Mount Mazama and the Crater Lake region, Oregon. Geological Society of America Bulletin, 118(11-12), pp.1331-1359.

Balco, G., Stone, J.O., Lifton, N.A. and Dunai, T.J., 2008. A complete and easily accessible means of calculating surface exposure ages or erosion rates from 10 Be and 26 Al measurements. Quaternary geochronology, 3(3), pp.174-195.

Bierman, P.R., 1994. Using in situ produced cosmogenic isotopes to estimate rates of landscape evolution: A review from the geomorphic perspective. *Journal of Geophysical Research: Solid Earth*, *99*(B7), pp.13885-13896.

Blackwelder, E., 1931. Pleistocene glaciation in the Sierra Nevada and basin ranges. *Geological Society of America Bulletin*, *42*(4), pp.865-922.

Blakely, R.J., Christiansen, R.L., Guffanti, M., Wells, R.E., Donnelly-Nolan, J.M., Muffler, L.P., Clynne, M.A. and Smith, J.G., 1997. Gravity anomalies, Quaternary vents, and Quaternary faults in the southern Cascade Range, Oregon and California: implications for arc and backarc evolution. *JOURNAL OF GEOPHYSICAL RESEARCH-ALL SERIES-*, *102*, pp.22-513.

Blard, P.H., Balco, G., Burnard, P.G., Farley, K.A., Fenton, C.R., Friedrich, R., Jull, A.T., Niedermann, S., Pik, R., Schaefer, J.M. and Scott, E.M., 2015. An inter-laboratory comparison of cosmogenic 3 He and radiogenic 4 He in the CRONUS-P pyroxene standard. Quaternary Geochronology, 26, pp.11-19.

Braunmiller, J., Nábělek, J., Leitner, B. and Qamar, A., 1995. The 1993 Klamath Falls, Oregon, earthquake sequence: Source mechanisms from regional data. Geophysical research letters, 22(2), pp.105-108.

Bursik, M., Renshaw, C., McCalpin, J. and Berry, M., 2003. A volcanotectonic cascade: Activation of range front faulting and eruptions by dike intrusion, Mono Basin-Long Valley Caldera, California. Journal of Geophysical Research: Solid Earth, 108(B8).

Carver, G.A., 1972, Glacial geology of the Mountain Lakes Wilderness and adjacent parts of the Cascade Range, Oregon [Ph.D. thesis]: Oregon State University, p. 25

Cerling, T.E., 1990. Dating geomorphologic surfaces using cosmogenic 3He. Quaternary Research, 33(2), pp.148-156.

Colman, S.M., Rosenbaum, J.G., Reynolds, R.L., and Sarna-Wojicicki, A.M., 2000, Post-Mazama (7 KA) Faulting Beneath Upper Klamath Lake, Oregon: Bulletin of the Seismological Society of America, v. 90, p. 243-247

Colman, S.M., Bradbury, J.P. and Rosenbaum, J.G., 2004. Paleolimnology and paleoclimate studies in Upper Klamath Lake, Oregon. Journal of Paleolimnology, 31(2), pp.129-138.

Cowgill, E., Gold, R.D., Xuanhua, C., Xiao-Feng, W., Arrowsmith, J.R. and Southon, J., 2009. Low Quaternary slip rate reconciles geodetic and geologic rates along the Altyn Tagh fault, northwestern Tibet. Geology, 37(7), pp.647-650.

Dicken, S.N., 1980. Pluvial Lake Modoc. *Klamath County, Oregon, and Modoc and Siskiyou Counties, California: Oregon Geology*, *42*(11), pp.179-187.

Dixon, T.H., Norabuena, E. and Hotaling, L., 2003. Paleoseismology and Global Positioning System: Earthquake-cycle effects and geodetic versus geologic fault slip rates in the Eastern California shear zone. Geology, 31(1), pp.55-58.

Dolan, J.F., Bowman, D.D. and Sammis, C.G., 2007. Long-range and long-term fault interactions in Southern California. Geology, 35(9), pp.855-858.

Dolan, J.F., McAuliffe, L.J., Rhodes, E.J., McGill, S.F. and Zinke, R., 2016. Extreme multi-millennial slip rate variations on the Garlock fault, California: Strain super-cycles, potentially time-variable fault strength, and implications for system-level earthquake occurrence. Earth and Planetary Science Letters, 446, pp.123-136.

Dreger, D., Ritsema, J. and Pasyanos, M., 1995. Broadband analysis of the 21 September, 1993 Klamath Falls earthquake sequence. Geophysical research letters, 22(8), pp.997-1000.

Frankel, K.L., Dolan, J.F., Finkel, R.C., Owen, L.A. and Hoeft, J.S., 2007. Spatial variations in slip rate along the Death Valley-Fish Lake Valley fault system determined from LiDAR topographic data and cosmogenic 10Be geochronology. Geophysical Research Letters, 34(18).

Friedrich, A.M., Wernicke, B.P., Niemi, N.A., Bennett, R.A. and Davis, J.L., 2003. Comparison of geodetic and geologic data from the Wasatch region, Utah, and implications for the spectral character of Earth deformation at periods of 10 to 10 million years. Journal of Geophysical Research: Solid Earth, 108(B4).

Gold, R.D. and Cowgill, E., 2011. Deriving fault-slip histories to test for secular variation in slip, with examples from the Kunlun and Awatere faults. Earth and Planetary Science Letters, 301(1), pp.52-64.

Gold, R.D., Cowgill, E., Arrowsmith, J.R., Chen, X., Sharp, W.D., Cooper, K.M. and Wang, X.F., 2011. Faulted terrace risers place new constraints on the late Quaternary slip rate for the central Altyn Tagh fault, northwest Tibet. Geological Society of America Bulletin, 123(5-6), pp.958-978.

Gosse, J.C. and Phillips, F.M., 2001. Terrestrial in situ cosmogenic nuclides: theory and application. Quaternary Science Reviews, 20(14), pp.1475-1560.

Hampel, A. and Hetzel, R., 2008. Slip reversals on active normal faults related to the inflation and deflation of magma chambers: Numerical modeling with application to the Yellowstone-Teton region. Geophysical Research Letters, 35(7).

Hawkins, F.F., Foley, L.L., and LaForge, R.C., 1989, Seismotectonic study for Fish Lake and Fourmile Lake dams, Rogue River Basin Project, Oregon, Volume 89-3: Denver, U.S. Bureau of Reclamation Seismotectonic Report, p. 26

Hetzel, R. and Hampel, A., 2005. Slip rate variations on normal faults during glacial–interglacial changes in surface loads. Nature, 435(7038), pp.81-84.

Liberty, L.M., Pratt, T.L., Lyle, M. and Madin, I.P., 2009. Neotectonic analysis of Upper Klamath Lake, Oregon: New insights from seismic reflection data. Geological Society of America Special Papers, 447, pp.71-82.

Licciardi, J.M., Clark, P.U., Brook, E.J., Elmore, D. and Sharma, P., 2004. Variable responses of western US glaciers during the last deglaciation. Geology, 32(1), pp.81-84.

Lifton, N., Sato, T. and Dunai, T.J., 2014. Scaling in situ cosmogenic nuclide production rates using analytical approximations to atmospheric cosmic-ray fluxes. Earth and Planetary Science Letters, 386, pp.149-160.

McCaffrey, R., King, R.W., Payne, S.J. and Lancaster, M., 2013. Active tectonics of northwestern US inferred from GPS-derived surface velocities. *Journal of Geophysical Research: Solid Earth*, *118*(2), pp.709-723.

Mueller, K., 2017. Variation in slip rates on active faults: Natural growth or stress transients?. *Geology*, *45*(3), pp.287-288.

Oskin, M., Perg, L., Shelef, E., Strane, M., Gurney, E., Singer, B. and Zhang, X., 2008. Elevated shear zone loading rate during an earthquake cluster in eastern California. Geology, 36(6), pp.507-510.

Peltzer, G., Crampé, F., Hensley, S. and Rosen, P., 2001. Transient strain accumulation and fault interaction in the Eastern California shear zone. Geology, 29(11), pp.975-978.

Pezzopane, S.K. and Weldon, R.J., 1993. Tectonic role of active faulting in central Oregon. Tectonics, 12(5), pp.1140-1169.

Phillips, F.M., Zreda, M., Plummer, M.A., Elmore, D. and Clark, D.H., 2009. Glacial geology and chronology of Bishop Creek and vicinity, eastern Sierra Nevada, California. Geological Society of America Bulletin, 121(7-8), pp.1013-1033.

Porter, S.C. and Swanson, T.W., 2008. 36Cl dating of the classic Pleistocene glacial record in the northeastern Cascade Range, Washington. American Journal of Science, 308(2), pp.130-166.

Priest, G.R., 1990. Volcanic and tectonic evolution of the Cascade volcanic arc, central Oregon. Journal of Geophysical Research: Solid Earth, 95(B12), pp.19583-19599.

Priest, G.R., Hladky, F.R., Mertzman, S.A., Murray, R.B. and Wiley, T.J., 2013. Volcanic signature of Basin and Range extension on the shrinking Cascade arc, Klamath Falls-Keno area, Oregon. Journal of Geophysical Research: Solid Earth, 118(8), pp.4013-4038.

Putkonen, J. and Swanson, T., 2003. Accuracy of cosmogenic ages for moraines. Quaternary Research, 59(2), pp.255-261.

Reid, H.F., 1910. The mechanics of the earthquake (Vol. 2). Carnegie institution of Washington.

Reynolds, R.L., Rosenbaum, J.G., Rapp, J., Kerwin, M.W., Platt Bradbury, J., Colman, S. and Adam, D., 2004. Record of late Pleistocene glaciation and deglaciation in the southern Cascade Range. I. Petrological evidence from lacustrine sediment in Upper Klamath Lake, southern Oregon. *Journal of Paleolimnology*, *31*(2), pp.217-233.

Rood, D.H., Burbank, D.W. and Finkel, R.C., 2011. Chronology of glaciations in the Sierra Nevada, California, from 10 Be surface exposure dating. Quaternary Science Reviews, 30(5), pp.646-661.

Rosenbaum, J.G., Reynolds, R.L., 2004, Record of Late Pleistocene glaciation and deglaciation in the southern Cascade Range. II. Flux of glacial flour in a sediment core from Upper Klamath Lake, Oregon: Journal of Paleolimnology, v. 31, p. 235-252

Sherrod, D.R. and Smith, J.G., 1990. Quaternary extrusion rates of the Cascade Range, northwestern United States and southern British Columbia. Journal of Geophysical Research: Solid Earth, 95(B12), pp.19465-19474.

Shimazaki, K. and Nakata, T., 1980. Time-predictable recurrence model for large earthquakes. Geophysical Research Letters, 7(4), pp.279-282.

Smith, J.G., 1988, Geologic Map of the Pelican Butte Quadrangle, Klamath, Oregon: U.S. Geologic Survey, scale 1: 62,500

Stewart, J.H., 1988. Tectonics of the Walker Lane belt, western Great Basin: Mesozoic and Cenozoic deformation in a zone of shear. Metamorphism and crustal evolution of the western United States, 7, pp.683-713.

Richard Styron (2015). Slip Rate Calculator, v. 0.1.2. Zenodo. doi:10.5281/zenodo.33360

Taylor, E.M., 1990. Volcanic history and tectonic development of the central High Cascade Range, Oregon. Journal of Geophysical Research: Solid Earth, 95(B12), pp.19611-19622.

Thompson, C.S., Weldon, R.J., Rubin, C.M., Abdrakhmatov, K., Molnar, P., Berger, G.W., 2002, Late Quaternary slip rates across the central Tien Shan, Kyrgyzstan, central Asia: Journal of Geophysical Research, vol. 107

Trench, D., Meigs, A. and Grunder, A., 2012. Termination of the northwestern Basin and Range province into a clockwise rotating region of transtension and volcanism, southeast Oregon. Journal of Structural Geology, 39, pp.52-65.

Troise, C., 2001. Stress changes associated with volcanic sources: Constraints on Kilauea rift dynamics. Journal of volcanology and geothermal research, 109(1), pp.191-203.

Unruh, J. and Humphrey, J., 2017. Seismogenic deformation between the Sierran microplate and Oregon Coast block, California, USA. *Geology*, *45*(5), pp.415-418.

Walter, T.R. and Amelung, F., 2004. Influence of volcanic activity at Mauna Loa, Hawaii, on earthquake occurrence in the Kaoiki Seismic Zone. Geophysical research letters, 31(7).

Walter, T.R., 2007. How a tectonic earthquake may wake up volcanoes: Stress transfer during the 1996 earthquake–eruption sequence at the Karymsky Volcanic Group, Kamchatka. Earth and Planetary Science Letters, 264(3), pp.347-359.

Wells, D.L., and Coppersmith, K.J., 1994, New empirical relationships among magnitude, rupture length, rupture width, rupture area, and surface displacement: Bulletin of the Seismological Society of America, v. 84, p. 974-1002

Wells, R.E., Weaver, C.S. and Blakely, R.J., 1998. Fore-arc migration in Cascadia and its neotectonic significance. Geology, 26(8), pp.759-762.

Wells, R.E. and McCaffrey, R., 2013. Steady rotation of the Cascade arc. Geology, 41(9), pp.1027-1030.

Wiley, T.J., Sherrod, D.R., Keefer, D.K., Qamar, A., Schuster, R.L., Dewey, J.W., Mabey, M.A., Black, G.L., and Wells, R.E., 1993, Klamath Falls earthquakes, September 20, 1993 - including the strongest quake ever measured in Oregon: Oregon Geology, v. 55, p. 127-134

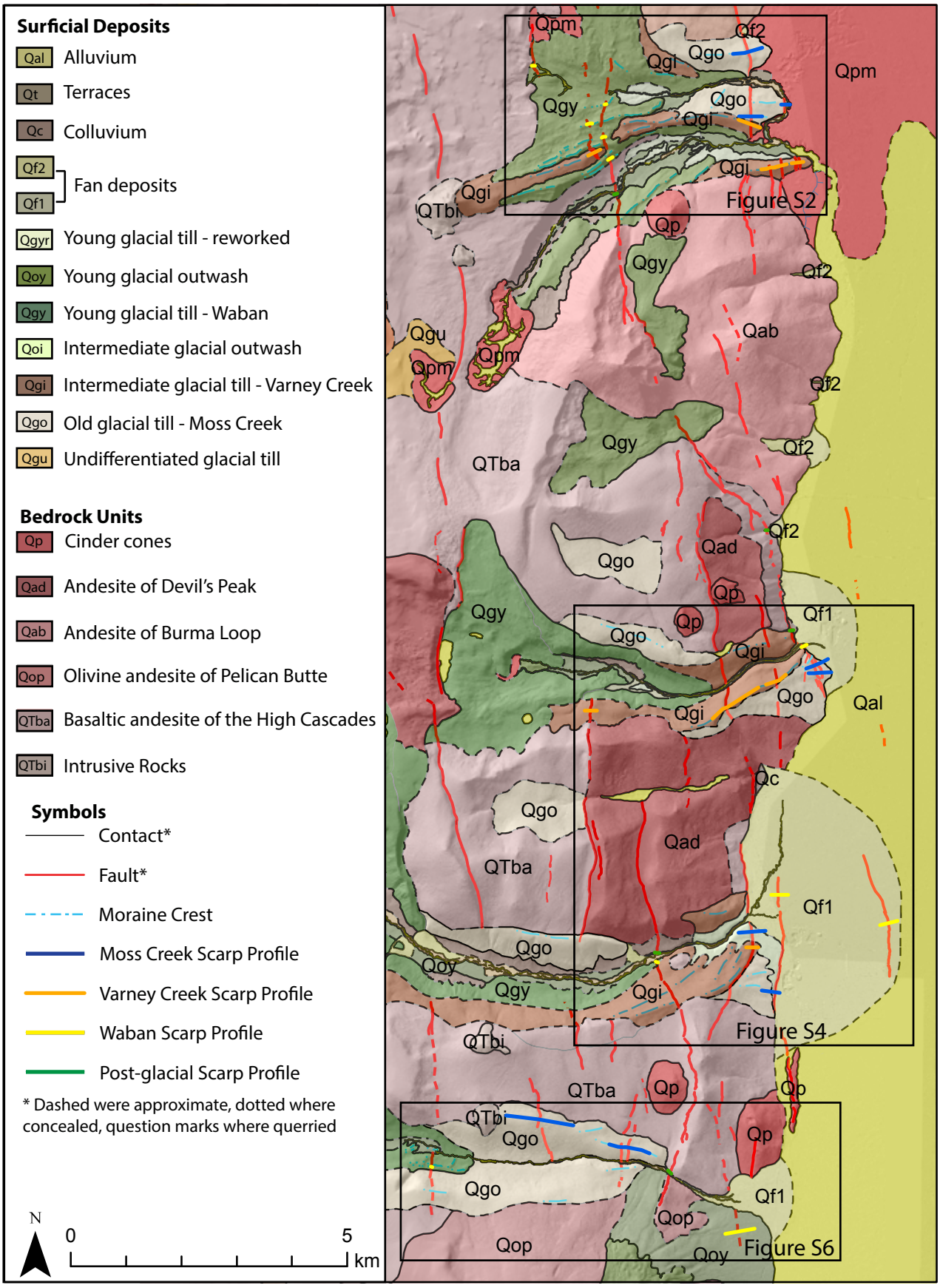

Supplementary figure 1 - Surficial geologic map of the WKLFZ on top of lidar hillshade highlighting fault scarp profile locations. Boxed areas are shown at finer scale in supplementary figures 2-4. Bedrcok mappin from Smith (1988).

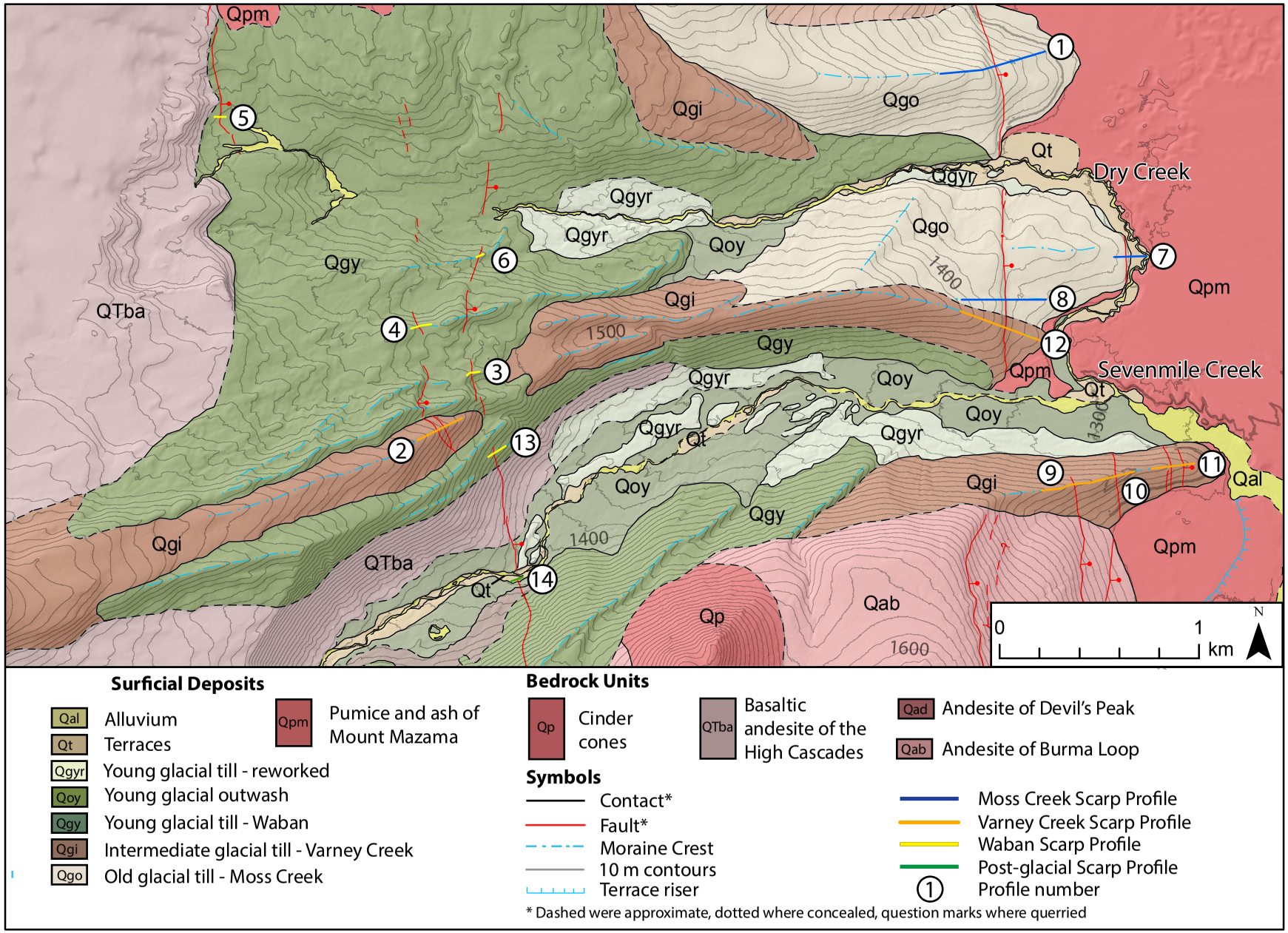

Supplementary Figure 2 - Surficical geologic map of Sevenmile and Dry Creeks over lidar bare earth hillshade available from the Oregon Department of Geology and Mineral Industries (DOGAMI). Bedrock mapping from Smith (1988). Scarp profile data reported in table 1. Profiles shown if supplementary figures 8 - 12.

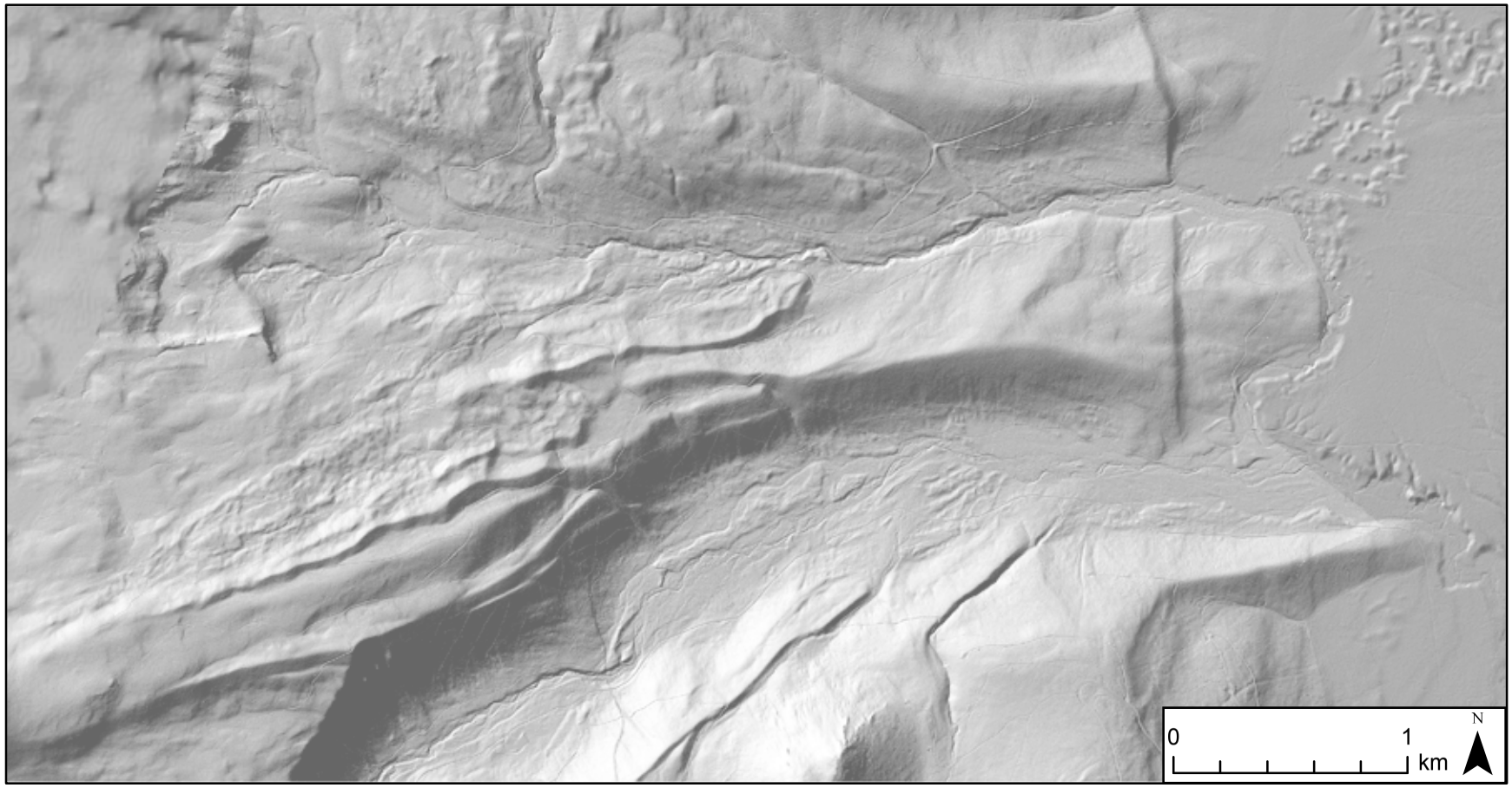

Supplementary Figure 3 - Uninterpreted lidar-derived bare earth hillshade of Sevenmile and Dry Creeks (supplementary figure 2) available from the Oregon Department of Geology and Mineral Industries (DOGAMI).

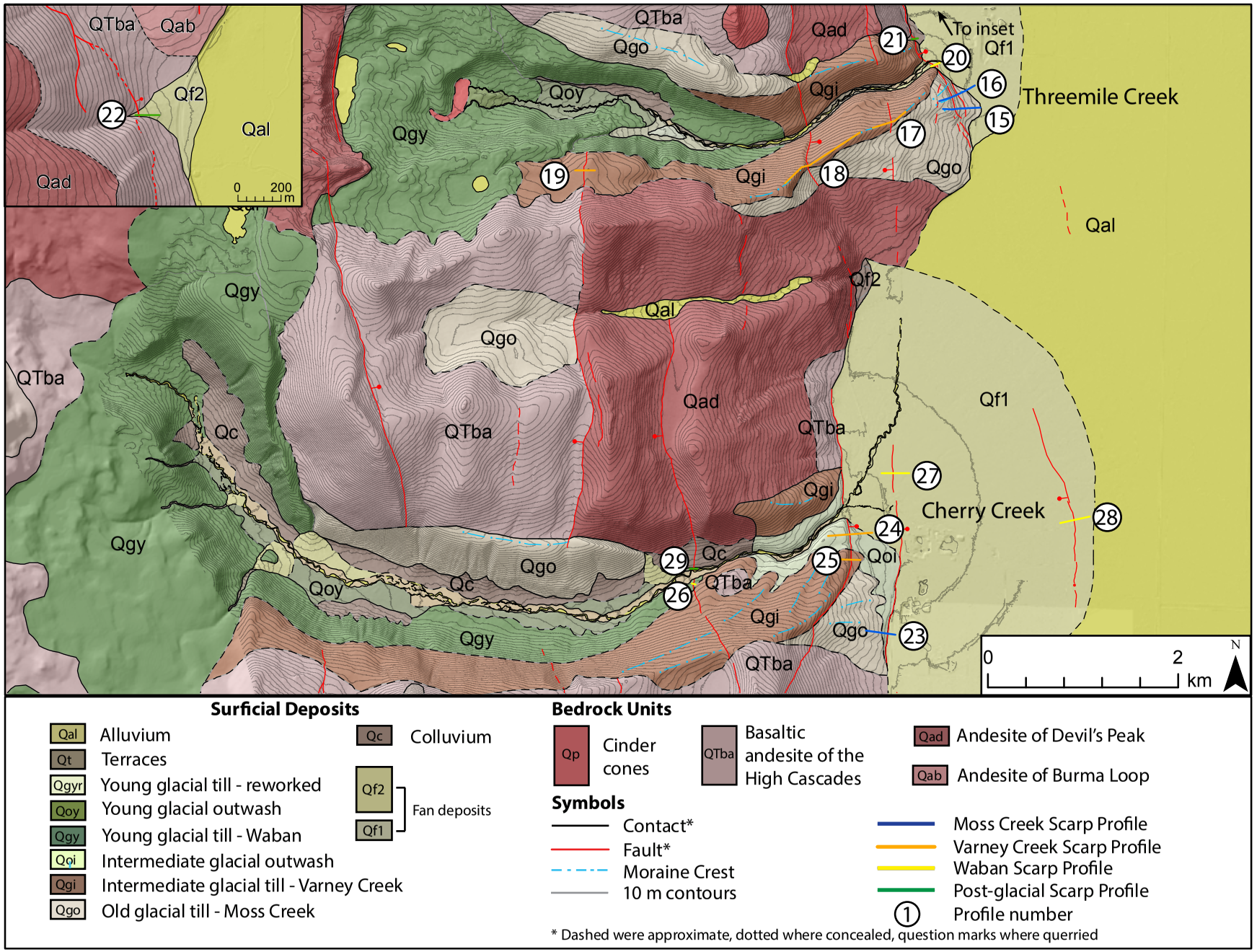

Supplementary figure 4 - Surficial geologic map of Threemile and Cherry Creeks over lidar bare earth hillshade available from DOGAMI. Inset - debris flow fan north of Threemile Creek. Bedrock mapping from Smith (1988). Scarp profile data reported in table 1. Profiles shown if supplementary figures 8 - 12.

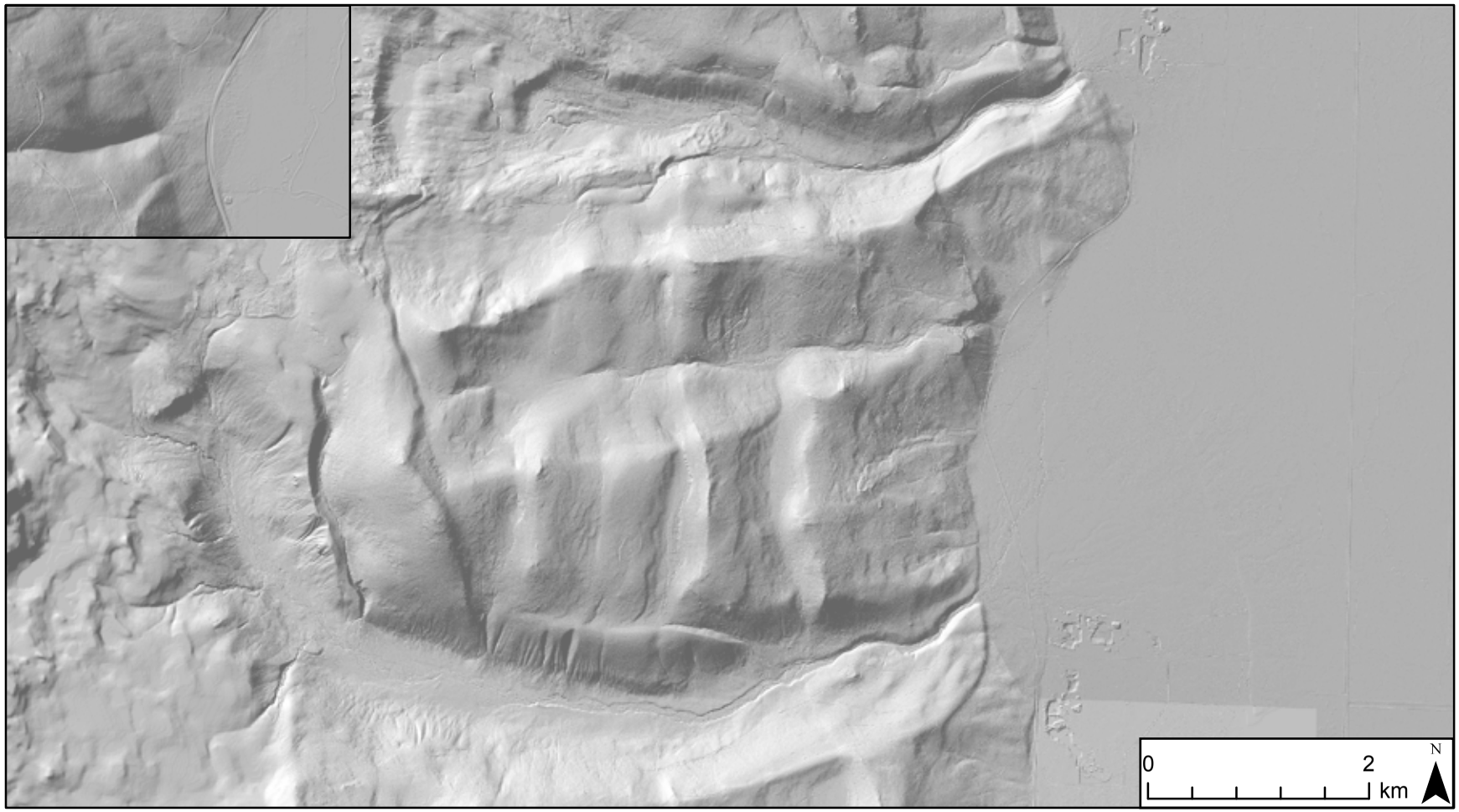

Supplementary figure 5 - Uninterpreted lidar-derived bare earth hillshade of Threemile and Cherry Creeks (supplementary figure 4) available from the Oregon Department of Geology and Mineral Industries (DOGAMI).

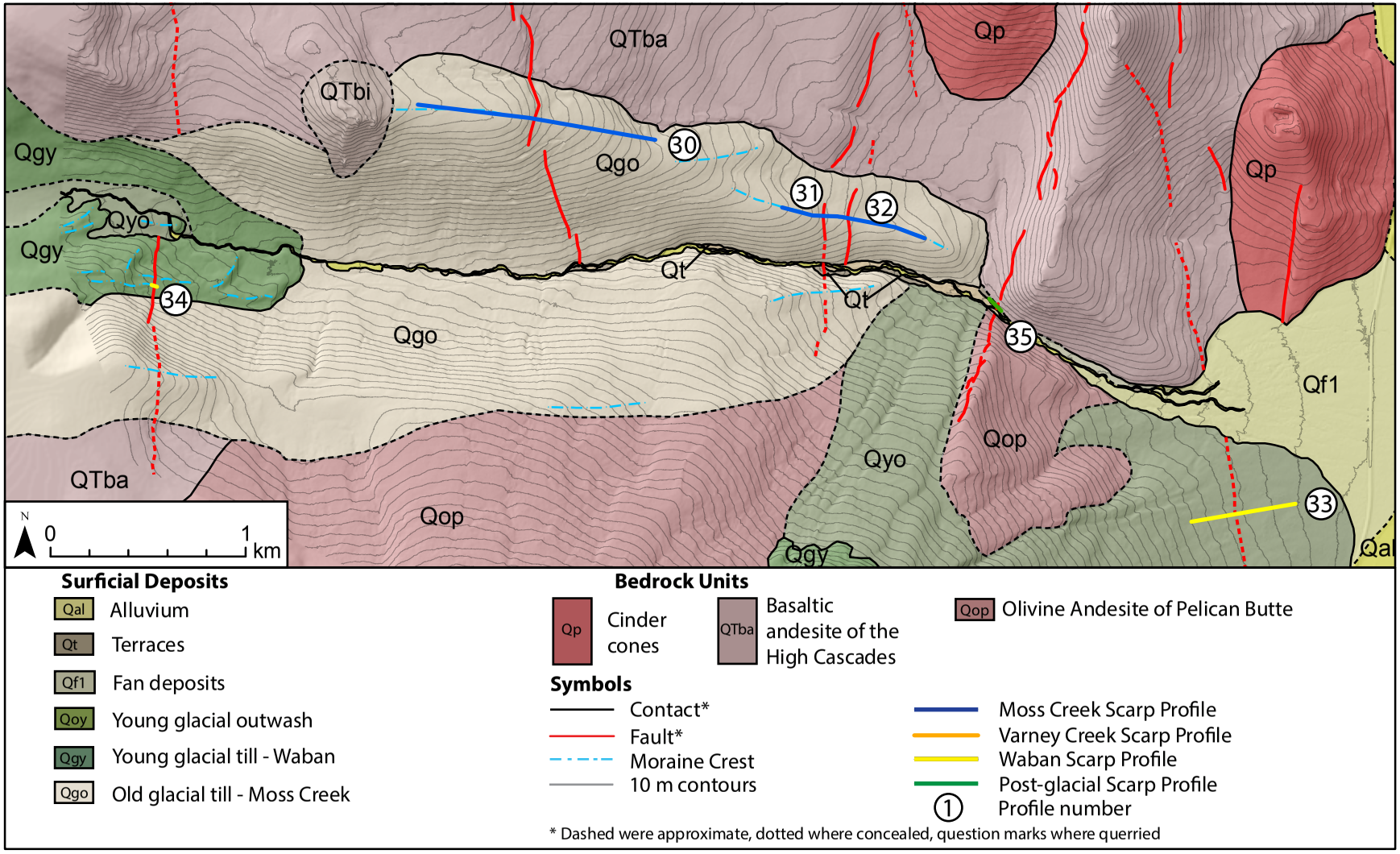

Supplementary figure 6 - Surficial geologic map of Rock Creek over lidar-derived bare earth hillshade available from DOGAMI. Location shown in supplementary figure 1. Bedrock mapping from Smith (1988). Scarp profile data reported in table 1. Scarp profiles shown in supplementary figures 8 -12.

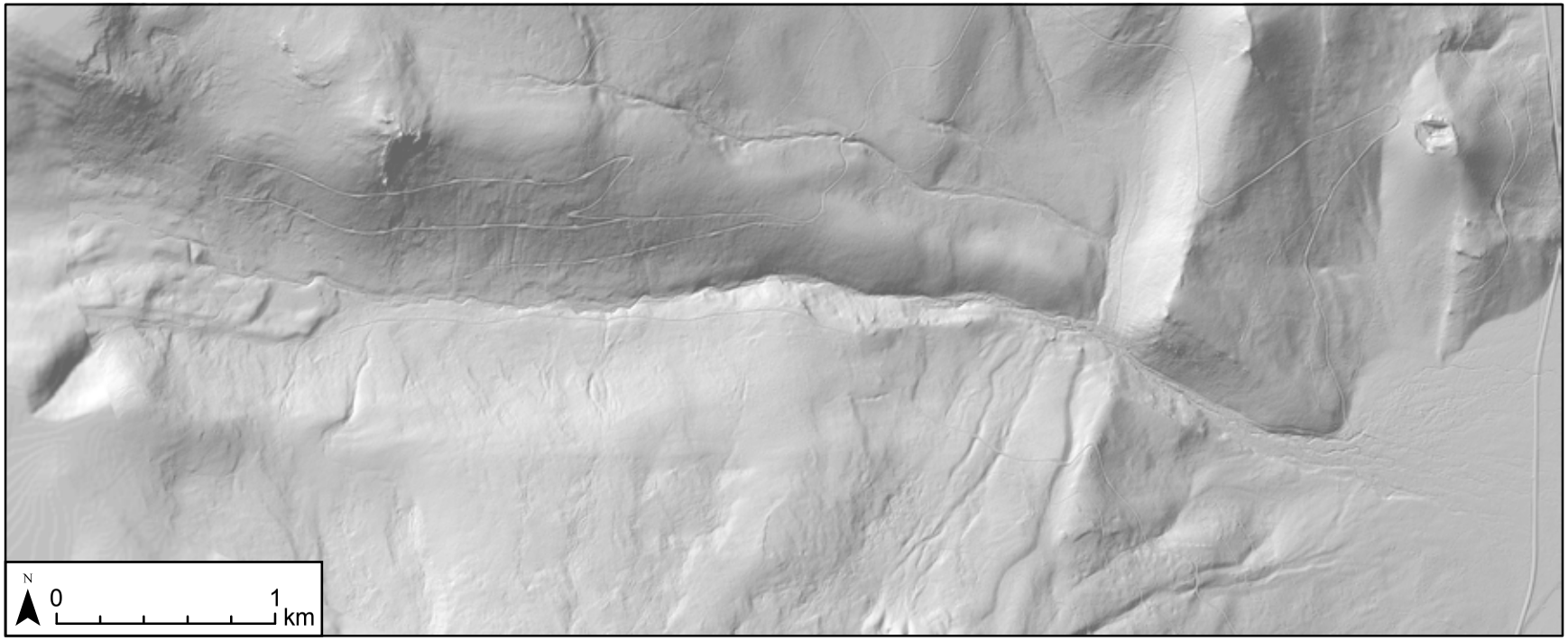

Supplementary figure 7 - Uninterpreted lidar-derived bare earth hillshade of Rock Creek (supplementary figure 6) available from the Oregon Department of Geology and Mineral Industries (DOGAMI).

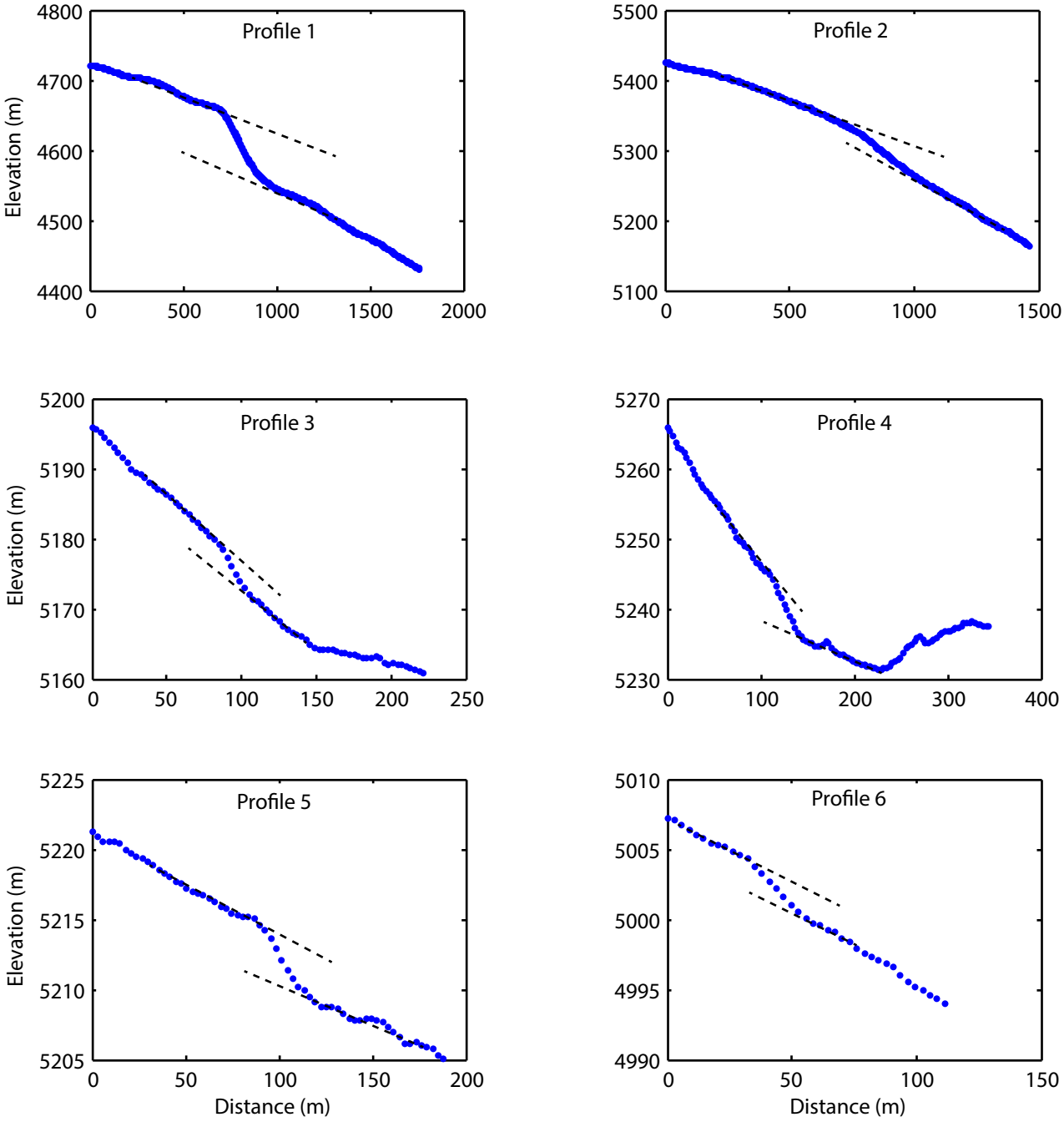

Supplementary Figure 8 - Scarp profiles measured at Dry Creek. Measurements summarized in supplementary table 1.

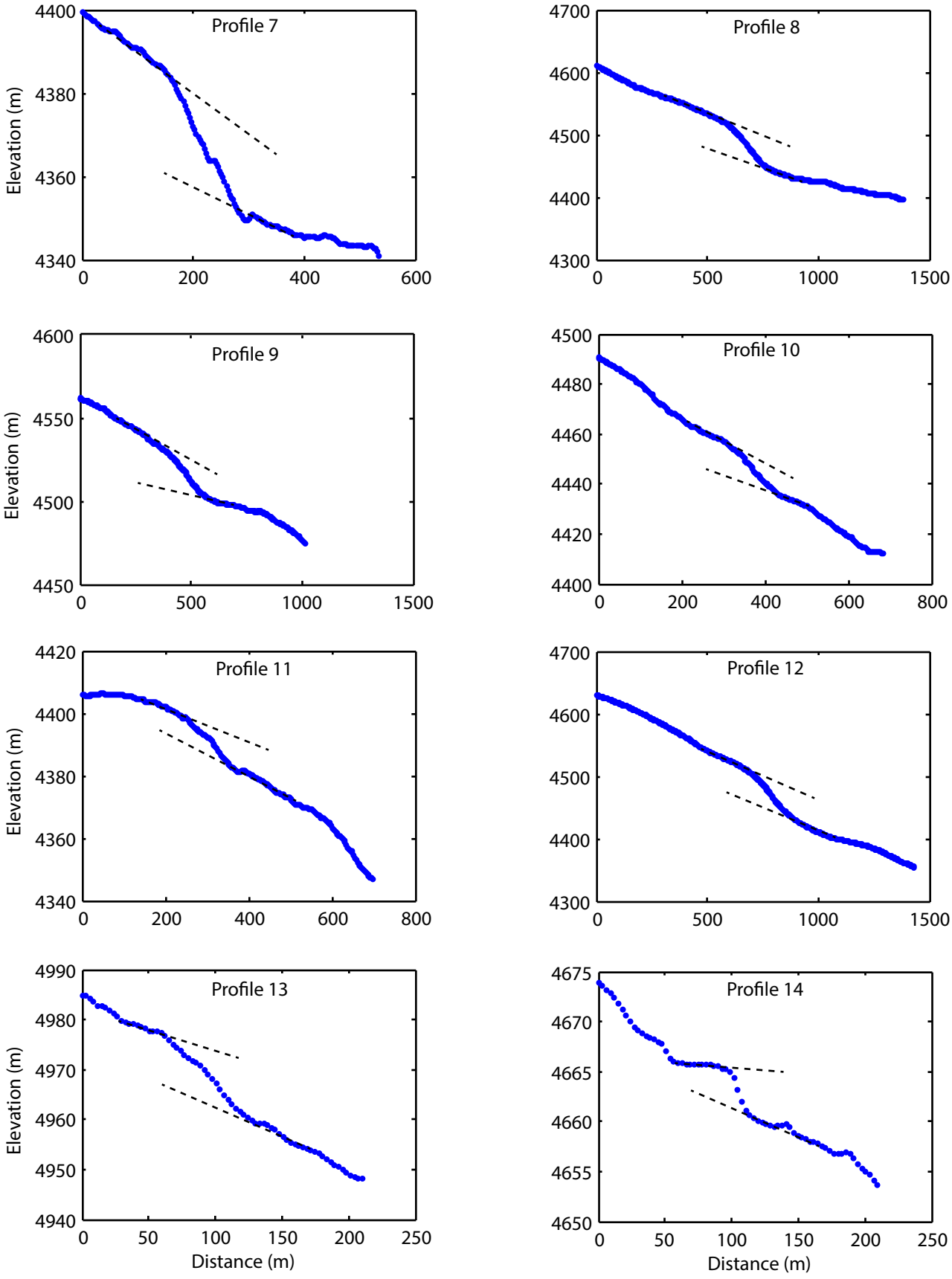

Supplementary Figure 9 - Scarp profiles measured at Sevenmile Creek. Measurements summarized in supplementary table 1.

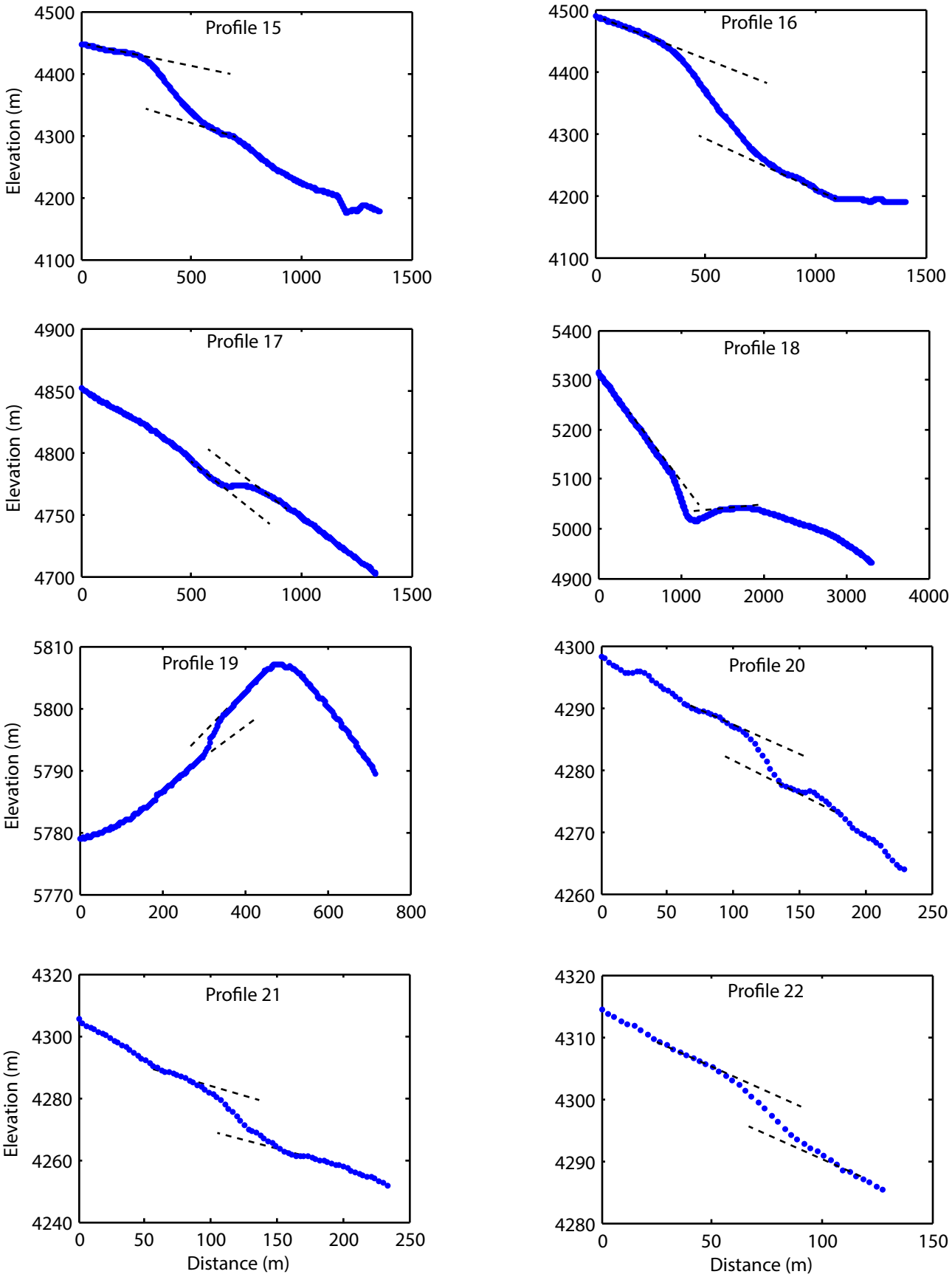

Supplementary Figure 10 - Scarp profiles measured at Threemile Creek. Measurements summarized in supplementary table 1.

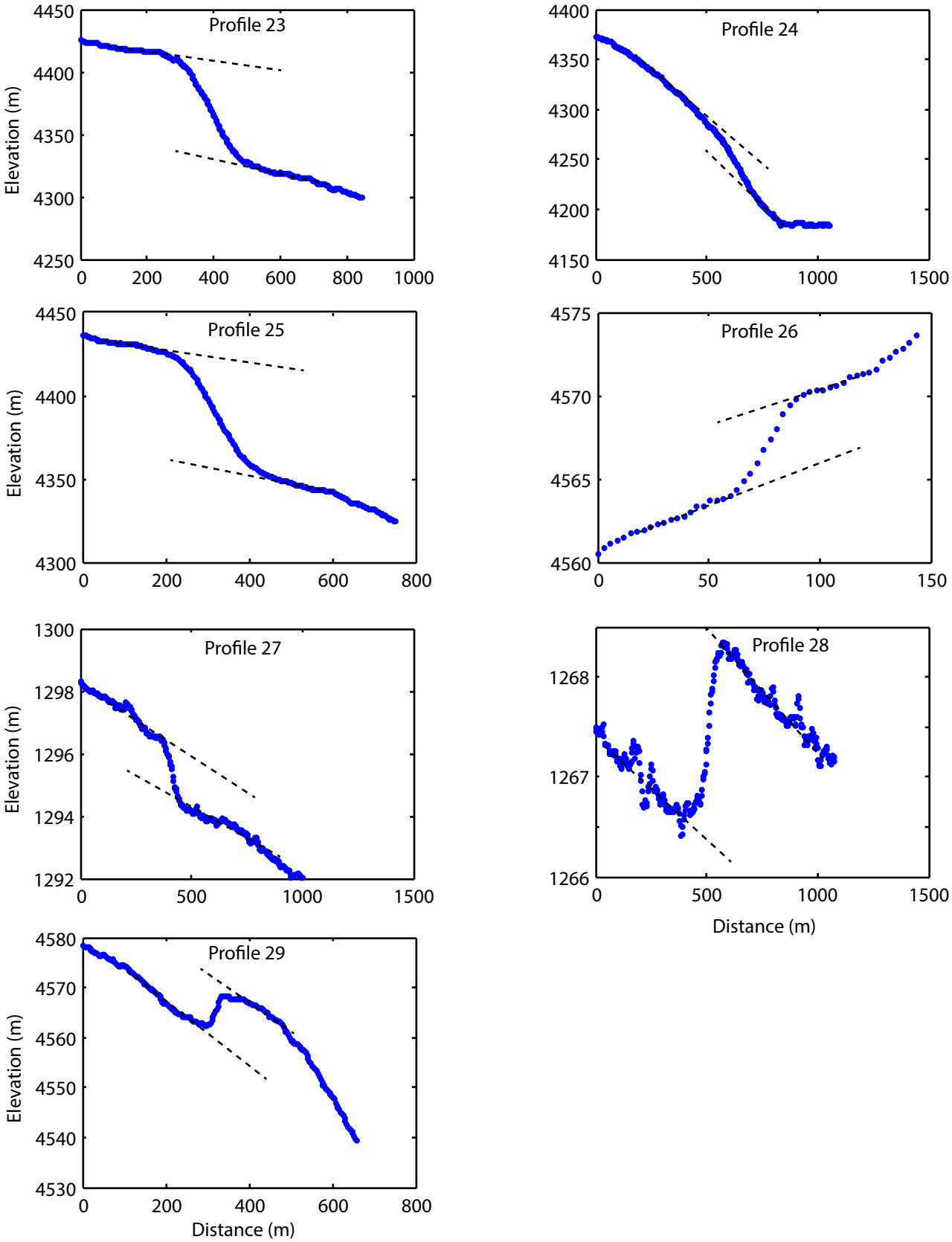

Supplementary Figure 11 - Scarp profiles measured at Cherry Creek. Measurements summarized in supplementary table 1.

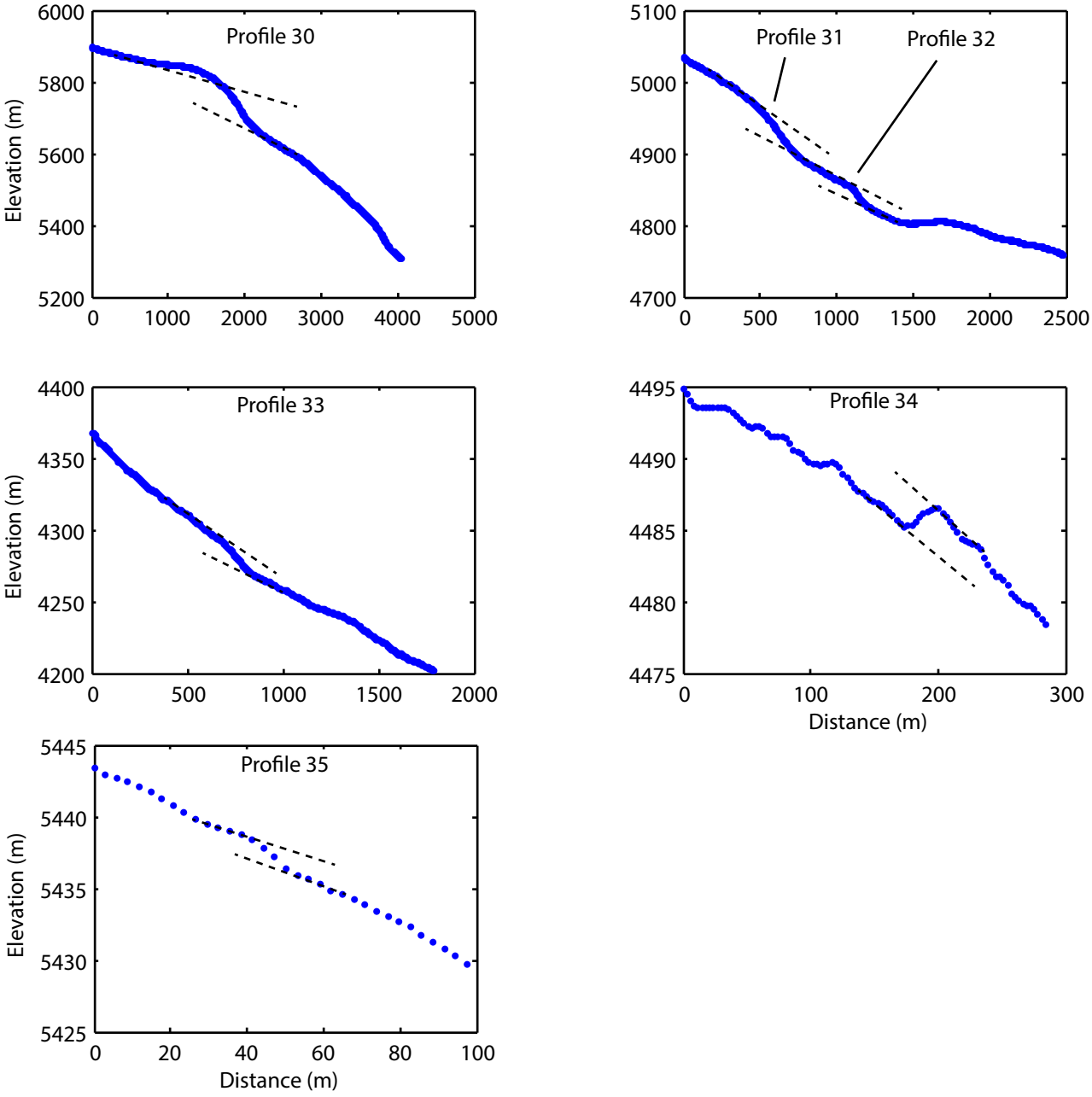

Supplementary Figure 12 - Scarp profiles measured at Rock Creek. Measurements summarized in supplementary table 1.

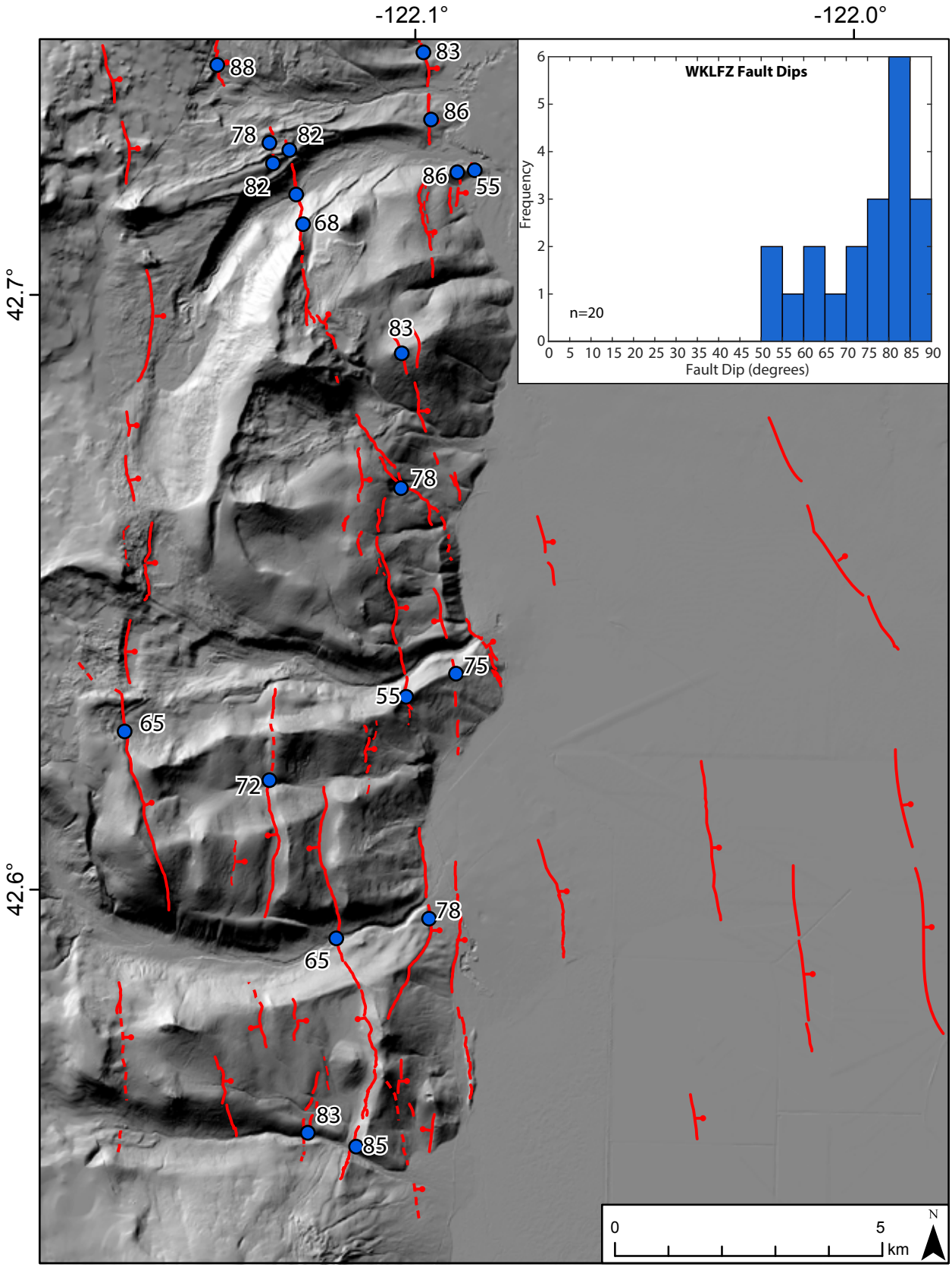

Supplementary Figure 13 - Fault dips determined by three point problems

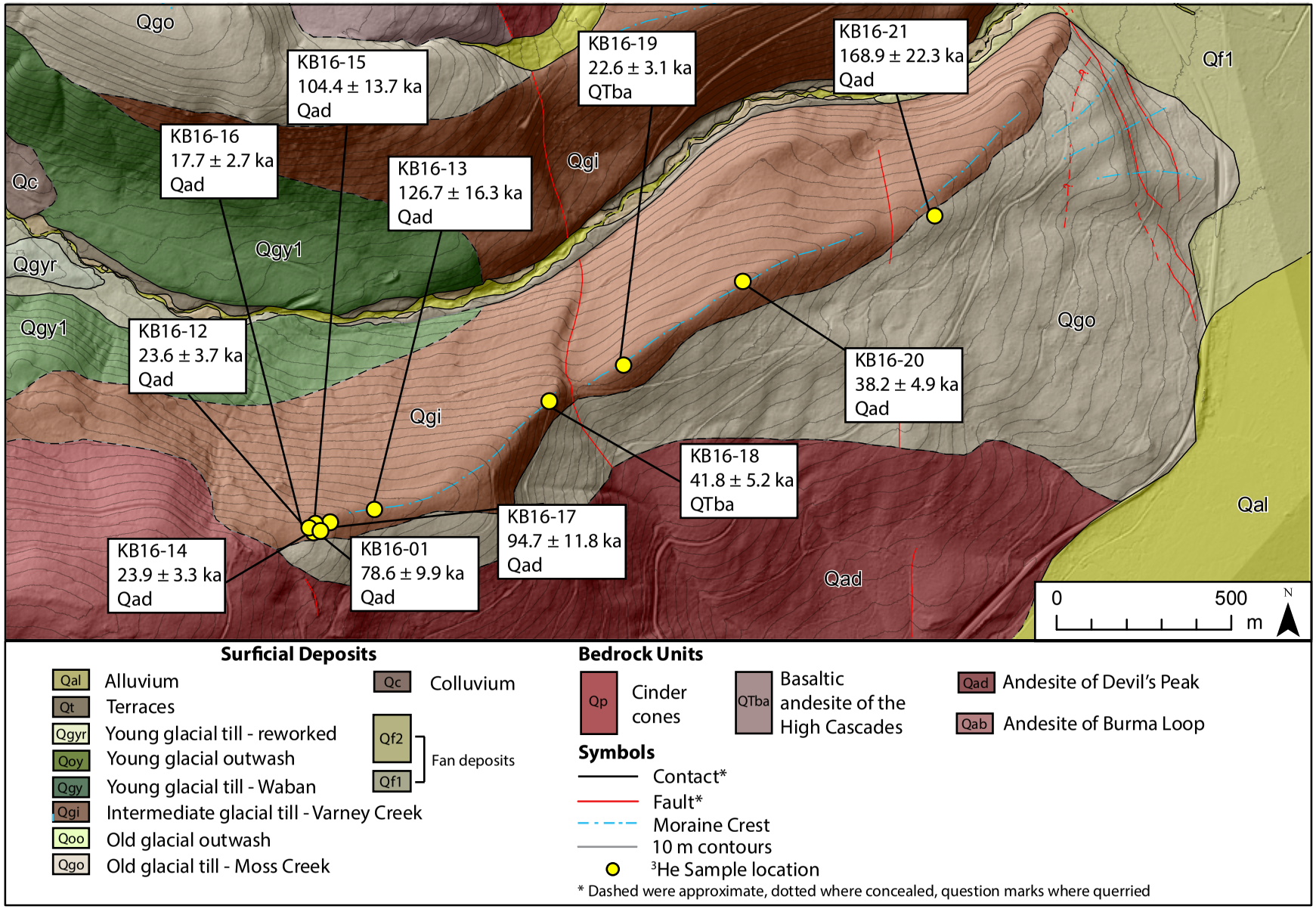

Supplementary Figure 14 - Sample location map for the Moss Creek/Varney Creek composite moraine at Threemile Creek

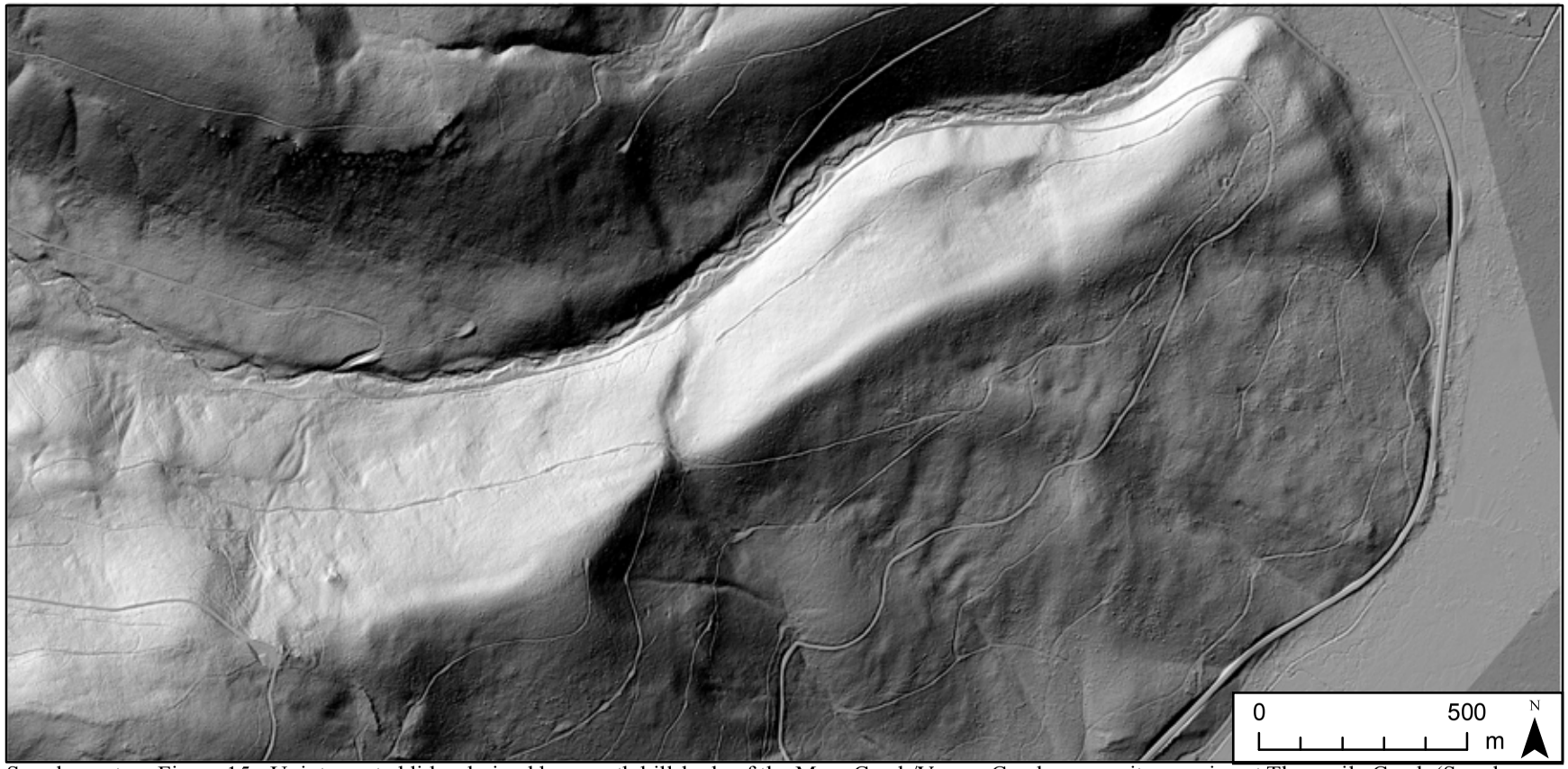

Supplementary Figure 15 - Uninterpreted lidar-derived bare earth hillshade of the Moss Creek/Varney Creek composite moraine at Threemile Creek (Supplementary figure 14) available from the Oregon Department of Geology and Mineral Industries.

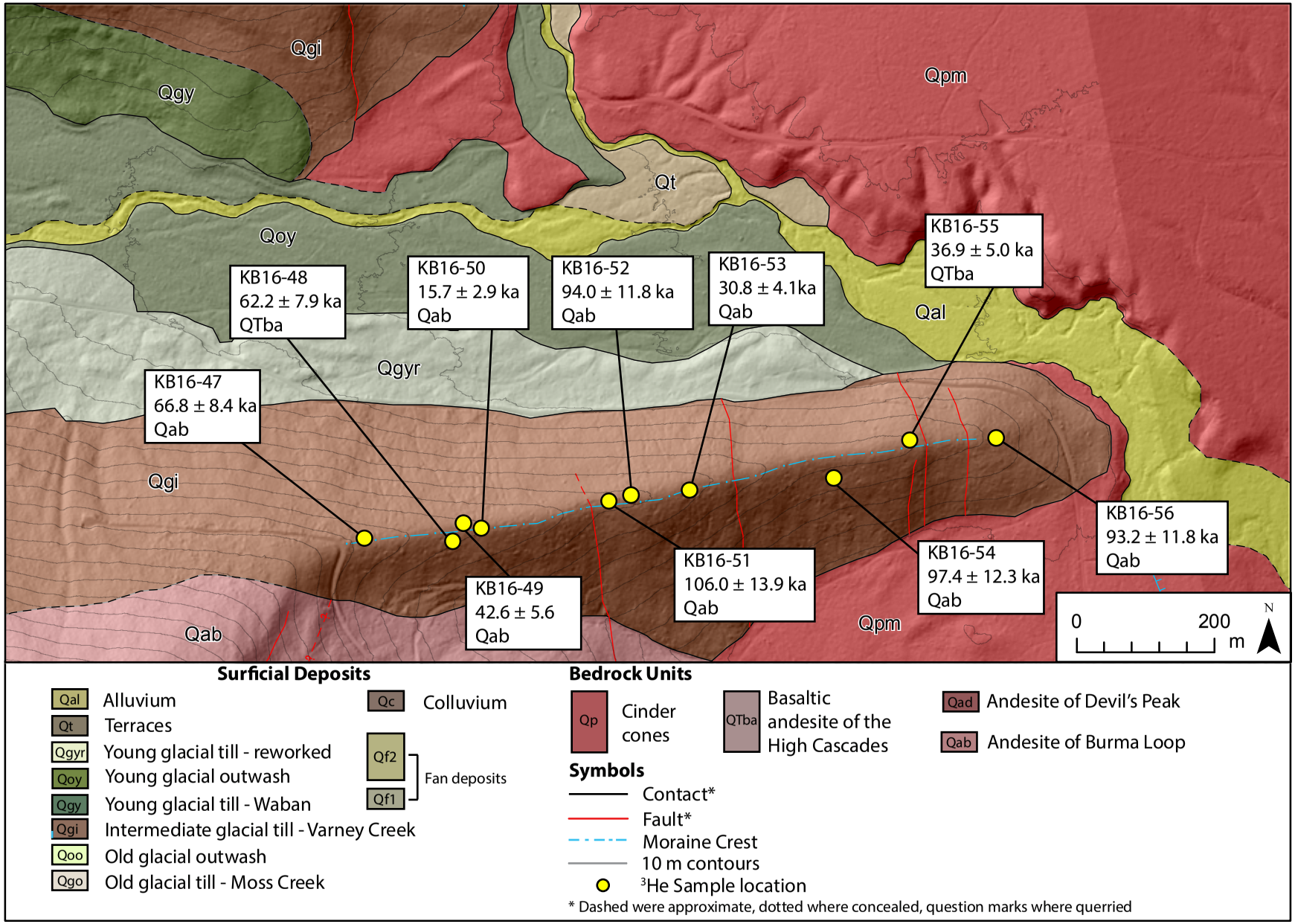

Supplementary Figure 16 - Sample location map for the Varney Creek moraine at Sevenmile Creek

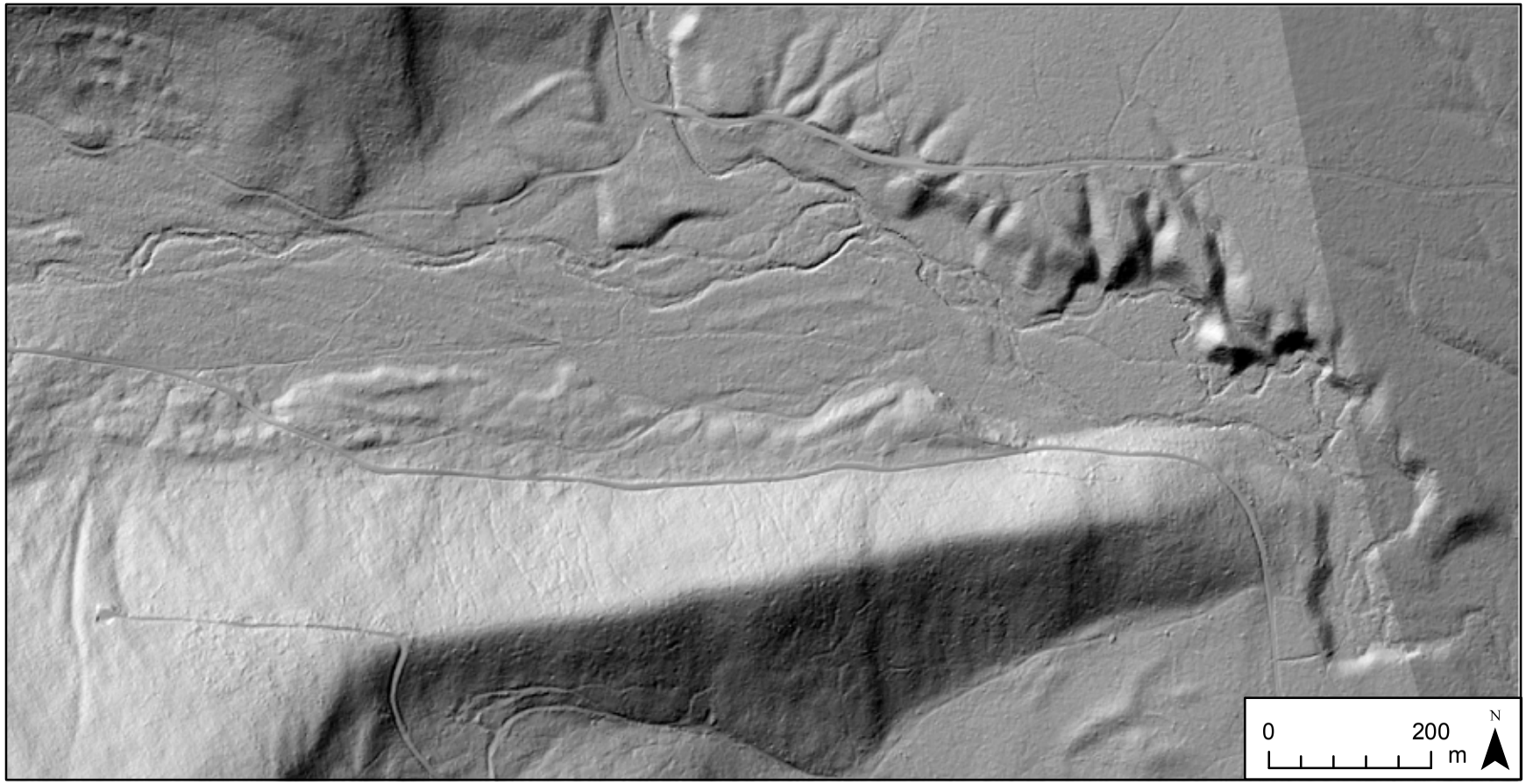

Supplementary Figure 17 - Uninterpreted lidar-derived bare earth hillshade of the Varney Creek moraine at Sevenmile Creek (Supplementary figure 15) available from the Oregon Department of Geology and Mineral Industries.

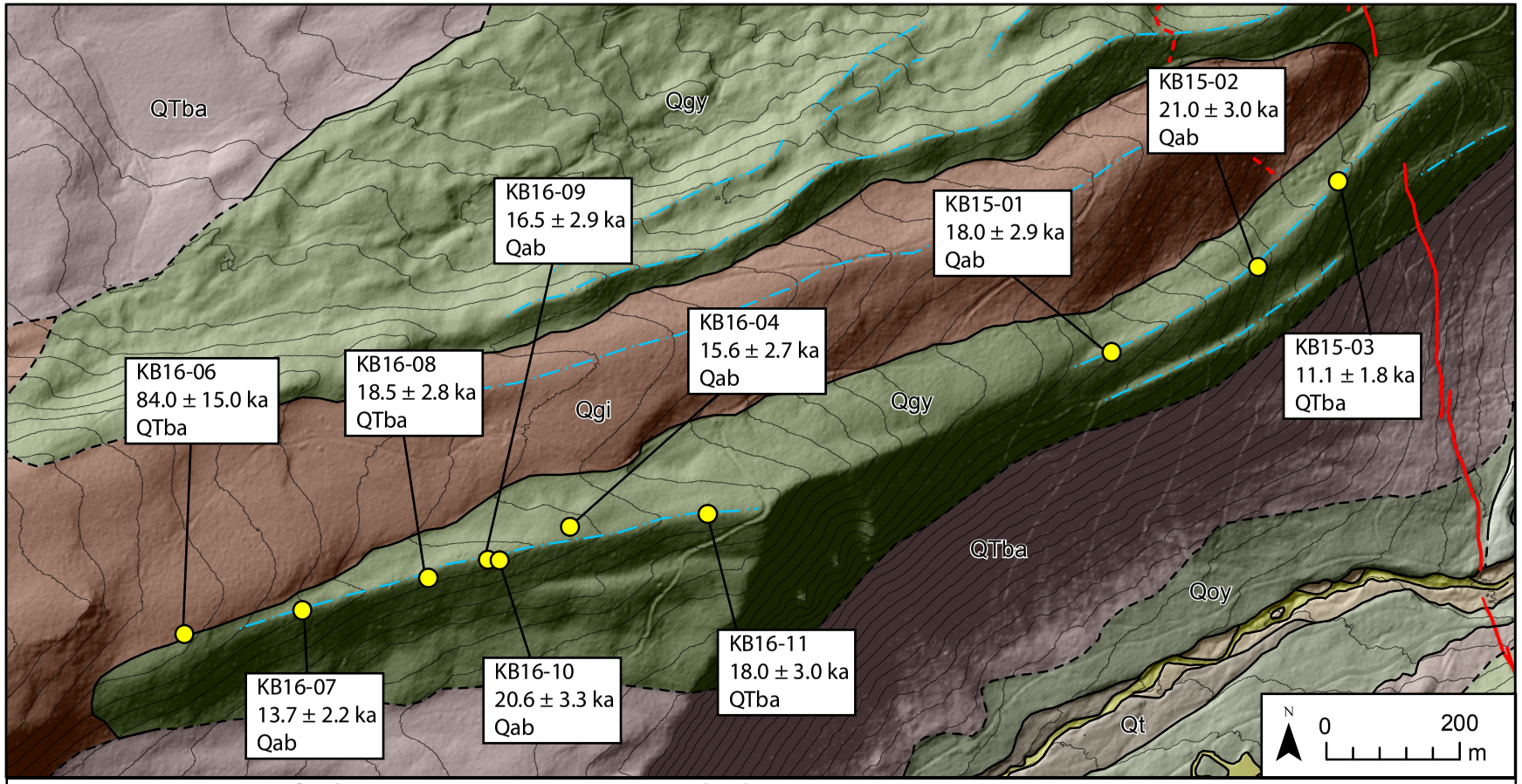

Supplementary Figure 18 - Sample location map for the Waban moraine at Sevenmile Creek

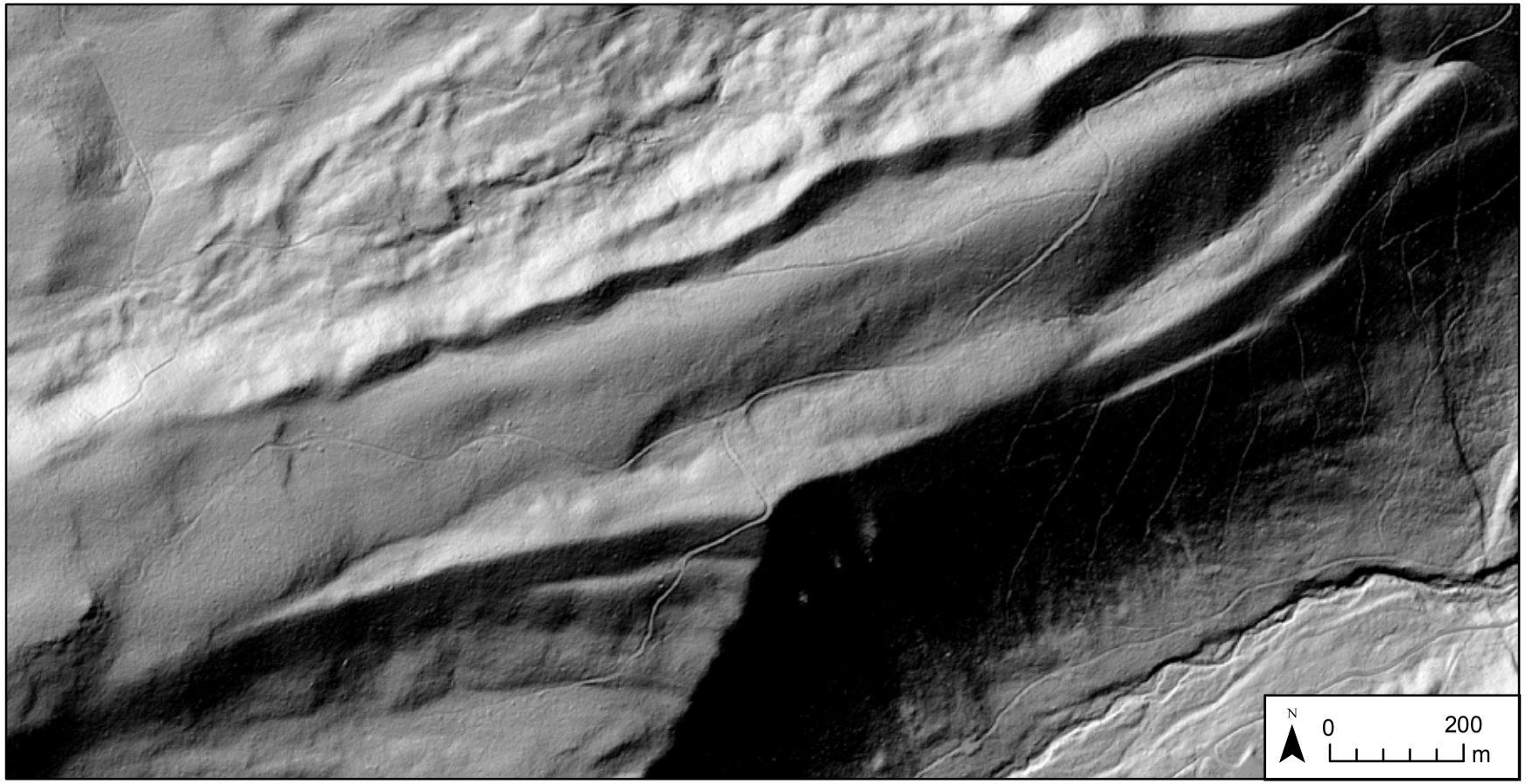

Supplementary Figure 19 - Uninterpreted lidar-derived bare earth hillshade of the Waban moraine at Sevenmile Creek (Supplementary figure 18) available from the Oregon Department of Geology and Mineral Industries.

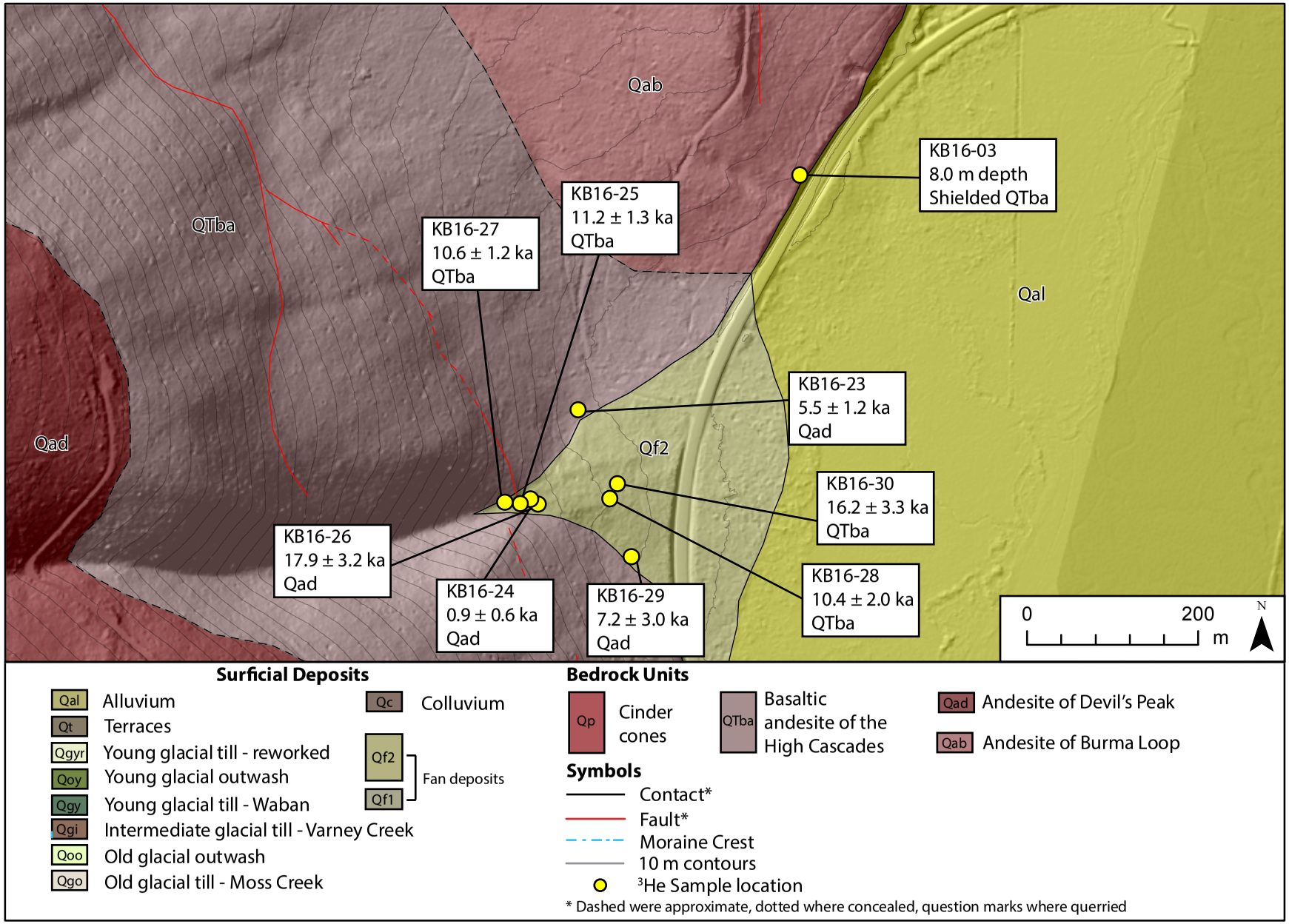

Supplementary Figure 2~~0~~ - Sample location map for the debris flow fan near Threemilemile Creek. Uninterpreted lidar hillshade is shown in supplementary figure 5 inset

Supplementary Figure 21 - Sampled boulders on the Moss Creek/Varney Creek moraine at Threemile Creek. Sample information detailed in Table 1.

Supplementary Figure 22 - Sampled boulders on the Moss Creek/Varney Creek moraine at Threemile Creek. Sample information detailed in Table 1.

Supplementary Figure 23 - Sampled boulders on the Moss Creek/Varney Creek moraine at Threemile Creek. Sample information detailed in Table 1.

Supplementary Figure 24 - Sampled boulders on the Moss Creek/Varney Creek moraine at Threemile Creek. Sample information detailed in Table 1.

Supplementary Figure 25 - Sampled boulders on the Moss Creek/Varney Creek moraine at Threemile Creek. Sample information detailed in Table 1.

Supplementary Figure 26 - Sampled boulder on the Moss Creek/Varney Creek moraine at Threemile Creek. Sample information detailed in Table 1.

Supplementary Figure 27 - Sampled boulder on the Moss Creek/Varney Creek moraine at Threemile Creek. Sample information detailed in Table 1.

Supplementary Figure 28 - Sampled boulders on the Varney Creek moraine at Sevenmile Creek. Sample information detailed in Table 1.

Supplementary Figure 29 - Sampled boulders on the Varney Creek moraine at Sevenmile Creek. Sample information detailed in Table 1.

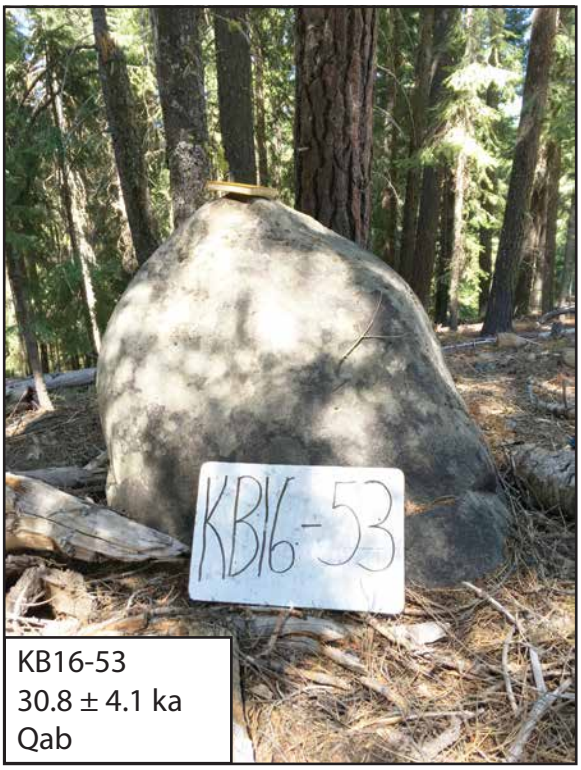

Supplementary Figure 30 - Sampled boulders on the Varney Creek moraine at Sevenmile Creek. Sample information detailed in Table 1.

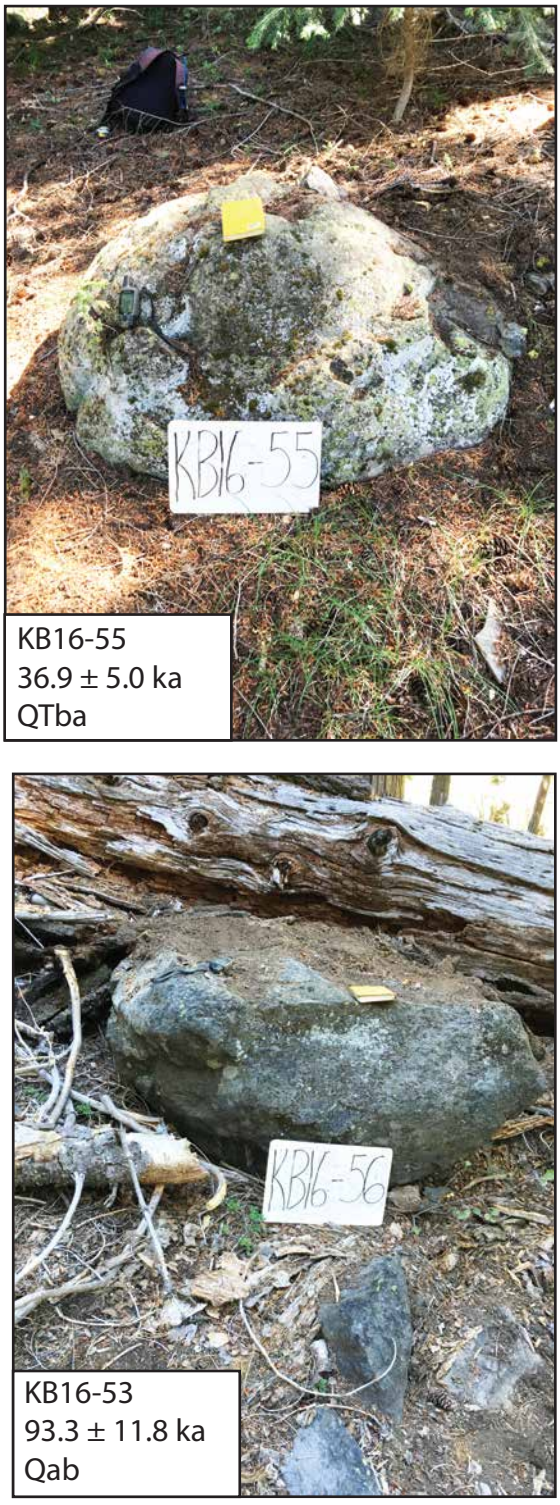

Supplementary Figure 31 - Sampled boulders on the Varney Creek moraine at Sevenmile Creek. Sample information detailed in Table 1.

Supplementary Figure 32 - Sampled boulders on the Waban moraine at Sevenmile Creek. Sample information detailed in Table 1.

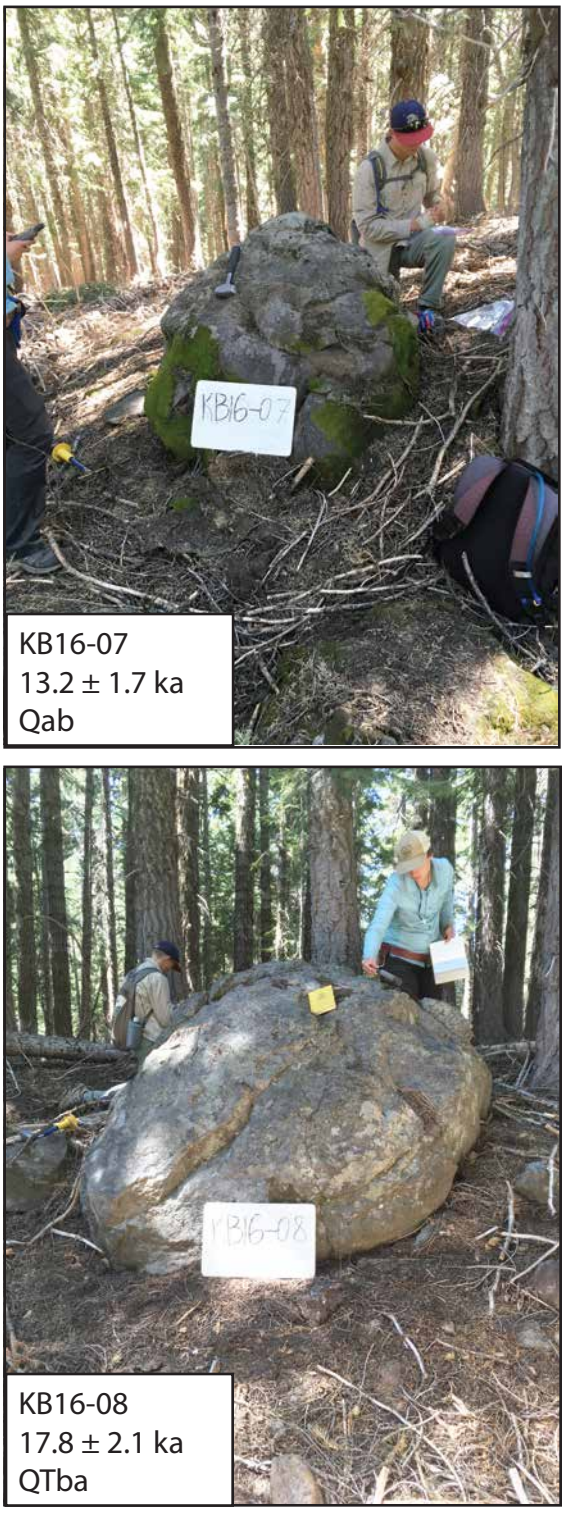

Supplementary Figure 33 - Sampled boulders on the Waban moraine at Sevenmile Creek. Sample information detailed in Table 1.

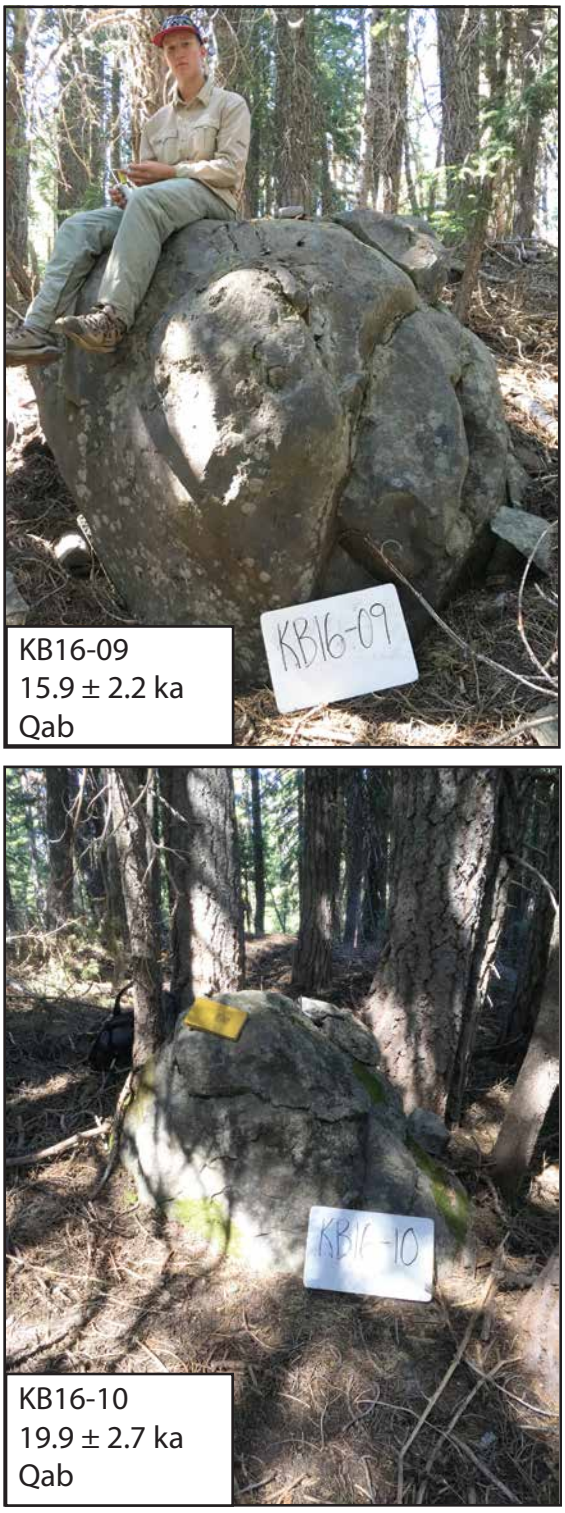

Supplementary Figure 34 - Sampled boulders on the Waban moraine at Sevenmile Creek. Sample information detailed in Table 1.

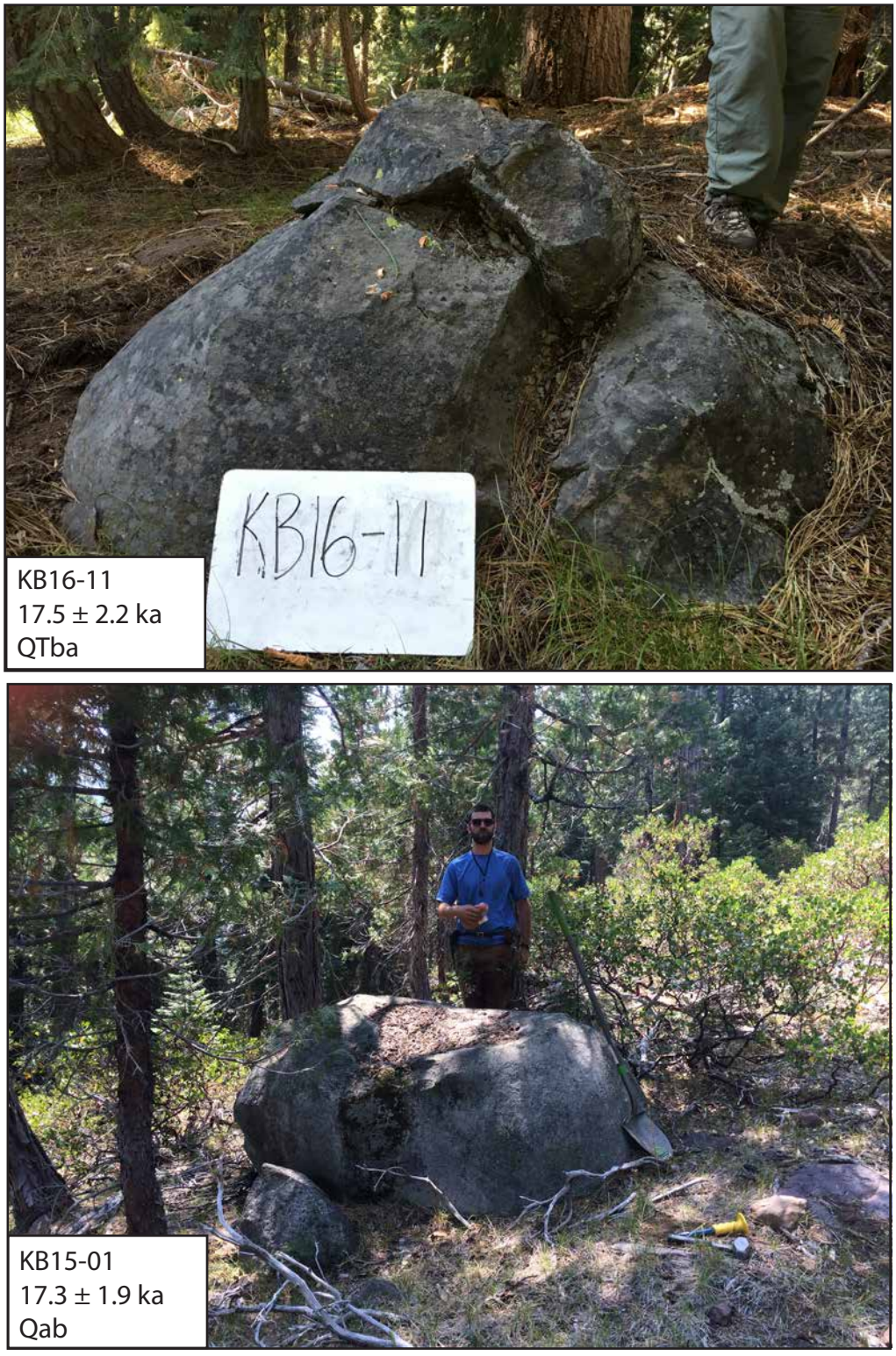

Supplementary Figure 35 - Sampled boulders on the Waban moraine at Sevenmile Creek. Sample information detailed in Table 1.

Supplementary Figure 36 - Sampled boulders on the Waban moraine at Sevenmile Creek. Sample information detailed in Table 1.

Supplementary Figure 37 - Sampled boulders on the debris flow fan near Threemile Creek. Sample information detailed in Table 1.

Supplementary Figure 38 - Sampled boulders on the debris flow fan near Threemile Creek. Sample information detailed in Table 1.

Supplementary Figure 39 - Sampled boulders on the debris flow fan near Threemile Creek. Sample information detailed in Table 1.

Supplementary Figure 40 - Sampled boulders on the debris flow fan near Threemile Creek. Sample information detailed in Table 1.

Supplementary Figure 41 - Depth profile from gravel quarry in Waban outwash fan at the mouth of Cherry Creek. Results shown in figure 6. See text for sample details